<div align="center">

Supplementary Information

"Force-velocity and tension transient measurements from *Drosophila* jump muscle reveal the necessity of both weakly-bound cross-bridges and series elasticity in models of muscle contraction"

</div>

<div align="center">

Katelyn J. Jarvis[a]**, Kaylyn M. Bell**[b]**, Amy K. Loya**[c]**, Douglas M. Swank**[b,c]**, Sam Walcott**[d]

[a] Department of Mathematics, University of California, Davis, CA
[b] Department of Bio. Sci., Center for Biotechnology and Interdisciplinary Studies, Rensselaer Polytechnic Institute, Troy, NY
[c] Department of Biomedical Engineering, Rensselaer Polytechnic Institute, Troy, NY
[d] Department of Mathematical Sciences, Worcester Polytechnic Institute, Worcester, MA

</div>

1 Modeling

1.1 Variable Definitions

Notation	Description
d	Power-stroke size
x	Extension of myosin molecule
κ	Stiffness of myosin
$k_B T$	Boltzmann's constant times temperature
δ	Parameter describing myosin's force-dependent chemistry
$E = \kappa \delta d / k_B T$	Non-dimensional parameter describing myosin's force-dependent chemistry
$v_{\max}$	Unloaded shortening velocity
$k_D(x)$	ADP release rate
k_D^0	Unloaded ADP release rate
$\mathcal{S}$	Length of stretch of half-sarcomere (nm) in a force-transient protocol
F_0	Isometric force
F_p	Force produced by a cross-bridge post-stretch in force-transient protocol
F_{nc}	Non-cross-bridge force present in force-transient measurement (same as F_{nc}^0 in supplement section 6.2)
$\eta_i(x,t)$	Probability density that myosin is bound in state i with an extension x
$N_i(t)$	Probability that myosin is in state i
$\kappa_w^+(x)$	Rate density for transition from unbound to bound states 5 to 1
$k_{w_0}^+$	Overall attachment rate
k_a, k_T, k_h^+, k_h^-	Rate constants for transition between states in kinetic scheme
[ATP]	ATP concentration
l, τ, V, $\hat{x}$, $\hat{\eta}$, L	Non-dimensional parameters for steady-state analytical solution (see section 1.3.2)
$G(x,\mu)$	Normalized Gaussian function in terms of x with mean μ (see section 1.4.2)
$\alpha_i(t)$, $\mu_i^j(t)$, $A(t)$, $b_i(t)$	Parameters for solving non-steady-state approximation (see section 1.4.2)
F_{xb}^0, F_{xb}^p	Cross-bridge forces pre- and post-stretch, respectively, in force transients (see section 6.2)
F_{nc}^0, F_{nc}^p	Non-cross-bridge forces pre- and post-stretch, respectively, in force transients (see section 6.2)
$V(x)$	Potential energy function

1.2   Mathematical Formulation of Model

In this section, we describe the mathematical implementation of the five-state model in Fig. 1B in the main text, and reproduced below in Fig. S1. The specific details of the four-state model are similar (see Walcott 2012 [1] for more detail). Myosin and actin interact in the cyclical pattern described by the kinetic scheme. Beginning with state 1, myosin is bound to actin in a pre-power-stroke form with ADP and inorganic phosphate (P_i) in its nucleotide binding site. In some order, myosin releases P_i and undergoes a conformational change, shifting to a post-power-stroke form with ADP still in the active site (state 2) . ADP is released in a force-dependent manner and actin and myosin stay bound in a post-power-stroke rigor state (state 3). ATP can then bind to the empty active site on myosin, causing dissociation of myosin from actin (state 4). Finally, ATP is hydrolyzed and myosin is unbound with ADP and P_i in the active site (state 5), and the cycle can begin again.
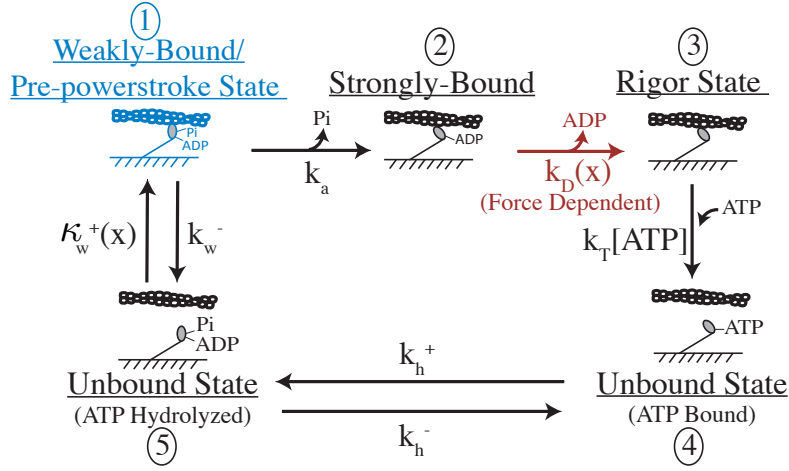
Figure S1: Five-state kinetic scheme detailing myosin's interaction with actin, including a weakly-bound state labeled in blue.

To transform this model into a system of equations, we must consider the force-dependence in the system. We use x to denote the molecular extension of a myosin molecule. When myosin is in an unbound state (states 4 and 5), it is not attached to actin, so there is no force on the molecule. Thus, the probability of being in one of these states is simply a function of time, denoted $N_i(t)$. However, when myosin is bound to actin, it is bound with a particular extension, x. Thus, for bound states (states 1, 2, and 3), we must define the probability density of myosin being bound in state i with an extension x as $\eta_i(x,t)$. The probability of being in one of the bound states is therefore $N_i(t) = \int_{-\infty}^{\infty} \eta_i(x,t)dx$.

We also must consider molecular extension when defining transitions between states. When myosin binds to actin, it does so with a particular extension. Thus, the transition from unbound to weakly bound (state 5 to state 1) must be defined as a rate density, $\kappa_w^+(x)$, giving an overall attachment rate of $k_{w_0}^+ = \int_{-\infty}^{\infty} \kappa_w^+(x)dx$. Additionally, ADP release rate (transition from state 2 to state 3) is dependent on force, and is therefore a function of molecular extension, $k_D(x)$.

Assuming a dense binding limit (i.e. that myosin can bind anywhere on the actin filament), a large number of cross-bridges, and the above notation, the five-state kinetic scheme can be expressed by

the following system of integro-PDEs:

$$\frac{\partial \eta_1}{\partial t} + v\frac{\partial \eta_1}{\partial x} = \kappa_w^+(x)N_5 - (k_w^- + k_a)\eta_1$$

$$\frac{\partial \eta_2}{\partial t} + v\frac{\partial \eta_2}{\partial x} = k_a\eta_1 - k_D(x)\eta_2$$

$$\frac{\partial \eta_3}{\partial t} + v\frac{\partial \eta_3}{\partial x} = k_D(x)\eta_2 - k_T[ATP]\eta_3 \tag{1}$$

$$\frac{dN_4}{dt} = k_T[ATP]\int_{-\infty}^{\infty} \eta_3 dx + k_h^- N_5 - k_h^+ N_4$$

$$\frac{dN_5}{dt} = \int_{-\infty}^{\infty} k_w^- \eta_1 dx + k_h^+ N_4 - \left(k_h^- + \int_{-\infty}^{\infty} \kappa_w^+(x)dx\right)N_5$$

$$1 = \int_{-\infty}^{\infty} \eta_1 dx + \int_{-\infty}^{\infty} \eta_2 dx + \int_{-\infty}^{\infty} \eta_3 dx + N_4 + N_5$$

where the final equation gives conservation of mass.

ADP release is dependent on molecular extension and, based on experimental measurements [2, 3, 4], we use the form:

$$k_D(x) = k_D^0 \exp\left(-\frac{\kappa(x+d)\delta}{k_B T}\right)$$

where k_D^0 is ADP release rate in the absence of force, κ is myosin's stiffness (assuming myosin acts as a linear spring), d is myosin's power-stroke size, $k_B T$ is Boltzmann's constant times temperature, and δ is a parameter, with units of distance, that describes myosin's force-dependent properties. Additionally, assuming that myosin's attachment probability varies exponentially with the energy required for myosin to bind with a given extension, we define the following rate density:

$$\kappa_w^+(x) = k_{w0}^+ \sqrt{\frac{\kappa}{2\pi k_B T}} \exp\left(-\frac{\kappa x^2}{2k_B T}\right)$$

All other rate constants (denoted k_w^-, k_a, k_T, k_h^-, k_h^+) are constant values.

With this, the mathematical model is described in full. Below, we detail the techniques used to solve this system under various conditions, resulting in expressions for $\eta_i(x,t)$ and $N_i(t)$. We can then calculate an expression for force. Force per myosin molecule is defined as the probability that myosin is in a force-producing state (states 1, 2, and 3), times the force it produces when bound. Noting that myosin has bound but has not undergone a power-stroke in state 1 (i.e. it has extension x), and has undergone a power-stroke of step size d in states 2 and 3 (i.e. it has extension $(x+d)$), we get the following calculation for force:

$$F = \int_{-\infty}^{\infty} \kappa\eta_1(x,t)x\,dx + \int_{-\infty}^{\infty} \kappa\eta_2(x,t)(x+d)dx + \int_{-\infty}^{\infty} \kappa\eta_3(x,t)(x+d)dx \tag{2}$$

3

In the following sections, we present both numerical solutions and analytical approximations for the system under various conditions. The numerical methods are important because they provide accurate and robust solutions to the system. However, they are often computationally expensive and inefficient. This makes optimization without a good initial guess time consuming, and sometimes impossible.

We develop analytical approximations to improve the optimization process. While less accurate, our approximations have two advantages. First, they give an efficient way to search parameter space. This allows us to quickly determine a good initial guess of best-fit parameters that can then be used with the less efficient, but more accurate, numerical solutions. Additionally, our analytical approximations provide intuition about our system, which is particularly useful when implementing the full model solutions.

1.3 Steady-State Solutions

To compare the model to force-velocity and energetics measurements, we must solve the system under steady-state conditions. First, we note that all of the experimental measurements we consider are done for conditions of high ATP concentration, $[ATP]$. The transition rate from state 3 to state 4 is dependent on this concentration, and thus, high concentrations of ATP results in a negligible population of cross-bridges in rigor. This allows us to simplify the system by assuming that myosin transitions directly from state 2 to state 4 at a rate of $k_D(x)$. With this simplification and the assumption of steady-state, the system in Eq. 1 becomes:

$$v\frac{d\eta_1}{dx} = -(k_w^- + k_a)\eta_1 + \left(\frac{k_w^- + k_a}{k_{w_0}^+}\right)\kappa_w^+(x)N_1 \tag{3}$$
$$v\frac{d\eta_2}{dx} = k_a\eta_1 - k_D(x)\eta_2$$

1.3.1 Numerical Solution for Steady-State

To numerically solve the system of ordinary differential equations (ODEs) in Eq. 3 for a given velocity value, v, we simultaneously implement a root find using Matlab's `fsolve` function and an ODE solver using Matlab's `ode15s`. We use the root find to determine the value of N_1 by solving $N_1 - \int_{-\infty}^{\infty} \eta_1(x)dx = 0$, and the ODE solver to find $\eta_1(x)$ and $\eta_2(x)$. We use a solver specialized for stiff ODEs because of the exponential term $(k_D(x))$, which becomes large at the boundary. We can then calculate the force using Eq. 2, resulting in a relationship for force as a function of velocity.

1.3.2 Analytical Solution for Steady-State

To solve for an analytical solution under steady-state conditions, it is most convenient to non-dimensionalize the system in Eq. 3. To do so, we define the following non-dimensional parameters: $\ell = \sqrt{2k_BT/\kappa}$, $\tau = 1/(k_w^- + k_a)$, $V = v\tau/\ell$, $\hat{x} = x/\ell$, $\hat{\eta} = \eta\ell$, $E = \kappa\delta d/k_BT$, $L = \ell/d$,

With this notation, the equation for η_1 becomes,

$$V\frac{\partial\hat{\eta}_1}{\partial\hat{x}} = -\hat{\eta}_1 + \frac{1}{\sqrt{\pi}}e^{-\hat{x}^2}N_1 \tag{4}$$

This can be analytically solved using an integrating factor. Using the convention that $v < 0$ for shortening, which therefore gives the boundary condition that $\hat{\eta}_1(\infty) = 0$, we get the solution,

$$\hat{\eta}_1 = \frac{N_1}{2V}e^{1/(4V^2)}e^{-\hat{x}/V}\left[-1 + \text{erf}\left(\hat{x} - \frac{1}{2V}\right)\right] \tag{5}$$

Next, we must solve for η_2. We implement the η_1 solution with the equation for η_2 in Eq. 3 to get,

$$v\frac{\partial\eta_2}{\partial x} = -k_D^0\exp\left(-EL\hat{x} - E\right)\eta_2 + \frac{k_a N_1}{2Vl}e^{1/(4V^2)}e^{-\hat{x}/V}\left[-1 + \text{erf}\left(\hat{x} - \frac{1}{2V}\right)\right] \tag{6}$$

To solve, we introduce a new non-dimensional length scale and rescale with $\overline{x} = x/d$ and $\overline{\eta_2} = d\eta_2$. Note that ℓ is small compared to d, so we can also define $L = \ell/d = \varepsilon$.

Finally, we define two non-dimensional parameters, $T_a = k_a\tau/\varepsilon$ and $T_d = k_D^0\tau/\varepsilon$. Both of these parameters include τ, the time scale of weak binding, which is assumed to be fast compared to strong binding. Thus, τ is $\mathcal{O}(\varepsilon)$, and T_a and T_d are both $\mathcal{O}(1)$. We can therefore simplify Eq. 6 to be,

$$\frac{\partial\overline{\eta_2}}{\partial\overline{x}} = \frac{-T_d}{V}\exp\left(-E\overline{x} - E\right)\overline{\eta_2} + \frac{T_a N_1}{V}\left[\frac{1}{2\varepsilon V}e^{1/(4V^2)}e^{-\overline{x}/(\varepsilon V)}\left(-1 + \text{erf}\left(\frac{\overline{x}}{\varepsilon} - \frac{1}{2V}\right)\right)\right] \tag{7}$$

We solve for η_2 using a matched asymptotic expansion. First, we construct the outer solution away from zero. In this region, we must solve,

$$\frac{\partial\overline{\eta_2}}{\partial\overline{x}} = \frac{-T_d}{V}\exp(-E\overline{x} - E)\overline{\eta_2} \tag{8}$$

which gives the solution,

$$\overline{\eta_2}^{\text{out}} = A\exp\left(\frac{T_d e^{-E\overline{x}-E}}{EV}\right) \tag{9}$$

Next, for the inner solution near zero, we must solve,

$$\frac{\partial\overline{\eta_2}}{\partial\overline{x}} = \frac{T_a N_1}{V}\left[\frac{1}{2\varepsilon V}e^{1/(4V^2)}e^{-\overline{x}/(\varepsilon V)}\left(-1 + \text{erf}\left(\frac{\overline{x}}{\varepsilon} - \frac{1}{2V}\right)\right)\right] \tag{10}$$

To solve, we must first define a layer coordinate to rescale into the layer. We divide the length parameter by ε, which we can write using our original notation: $\overline{x}/\varepsilon = \hat{x}$. Rescaling Eq. 10 allows us to solve for the inner solution with an arbitrary constant. Noting that $\overline{\eta_2}^{\text{in}}(\infty) = 0$, we can solve for this constant to get the solution

$$\overline{\eta_2}^{\text{in}} = \frac{T_a N_1}{2V}\left(\text{erf}(\hat{x}) + e^{1/(4V^2)}e^{-\hat{x}/V}\left(1 + \text{erf}\left(\frac{1}{2V} - \hat{x}\right)\right) - 1\right) \tag{11}$$

5

Matching these solutions near zero, we get the following composite solution:

$$\eta_2^{\text{comp}} = \begin{cases} \eta_2^{\text{in}} & \forall x, \hat{x}, \overline{x} \\ \eta_2^{\text{in}} + \eta_2^{\text{out}} - \eta_2^{\text{match}} & \text{for } x, \hat{x}, \overline{x} < 0 \end{cases}$$

where

$$\eta_2^{\text{out}} = \frac{-T_a N_1}{V} \exp\left(\frac{-T_d e^{-E}}{EV}\right) \exp\left(\frac{T_d e^{-E\overline{x}-E}}{EV}\right)$$

$$\eta_2^{\text{in}} = \frac{T_a N_1}{2V}\left(\text{erf}(\hat{x}) + e^{1/(4V^2)} e^{-\hat{x}/V}\left(1 + \text{erf}\left(\frac{1}{2V} - \hat{x}\right)\right) - 1\right) \tag{12}$$

$$\eta_2^{\text{match}} = \frac{-T_a N_1}{V}$$

This expression for η_2 can be integrated to solve for N_2, since $N_2 = \int_{-\infty}^{\infty} \eta_2(x,t)dx$. A value for N_2 then allows us to solve for N_1.

Combining all of the above, we have fully defined analytical expressions for η_1 and η_2. As a final step, we can use Eq. 2 to solve for force as a function of shortening velocity.

1.4 Non-Steady-State Solutions

In the force transient experiments, the muscle fiber is activated and held isometrically, stretched on a very rapid time scale, and then held isometrically again. Therefore, to compare the model to these measurements, we assume isometric conditions and solve for force as a function of time.

Again, we assume conditions of high ATP, reducing our five-state model to not include the negligibly populated state 3. Additionally assuming isometric conditions (i.e. $v = 0$), the system (Eq.1) reduces to the following:

$$\frac{\partial \eta_1}{\partial t} = \kappa_w^+(x)N_5 - (k_w^- + k_a)\eta_1$$
$$\frac{\partial \eta_2}{\partial t} = k_a\eta_1 - k_D(x)\eta_2 \tag{13}$$
$$\frac{dN_5}{dt} = k_w^- N_1 + k_h^+(1 - N_1 - N_2 - N_5) - (k_h^- + k_{w0}^+)N_5$$

1.4.1 Numerical Solution for Non-Steady-State

To numerically solve the system, we use the method of characteristics to convert these partial differential equations (PDEs) to a system of ODEs at each x. We then implement a fourth-order Runge-Kutta algorithm (RK4) in Matlab to solve the system of ODEs. We implement our own RK4 instead of using one of Matlab's suite of ODE solvers because of the integral constraint,

$N_i = \int_{-\infty}^{\infty} \eta_i(x,t)dx$. This constraint results in coupling between the characteristics, so that the ODEs are coupled and cannot be solved individually.

To implement RK4, we first solve the system analytically in steady-state ($t = 0$). Our simulation begins at the time of stretch, and so the initial condition is the steady-state distributions shifted by the stretch amplitude. For each value of x, we have a system of ODEs. We use the RK4 algorithm to take a step forward in time, using the values of η_1, η_2, N_1, N_2 and N_5 at the previous time step, to solve for the values of η_1, η_2 and N_5 at the next point in time. After the time step, we integrate the new distributions for η_1 and η_2 to get the new N_1 and N_2 values. Repeating this process, our final result is $\eta_1(x,t)$ and $\eta_2(x,t)$, and we can use Eq. 2 to solve for $F(t)$.

1.4.2   Analytical Approximation for Non-Steady-State

Given both the x and t-dependence in the non-steady-state system (Eq. 13), this system cannot be solved analytically. Instead, we develop the following moment approximation [5], which allows us to approximate the system of PDEs as a set of ODEs, which we can then optimize with greater efficiency.

Recall that $\eta_1(x,t)$ and $\eta_2(x,t)$ are the probability densities that myosin is weakly or strongly-bound, respectively, with a particular extension, x at time t. We assume the attachment rate varies exponentially with the energy required for myosin to bind with a particular extension, which means that the attachment rate is a normalized Gaussian function centered at 0. Thus, myosin molecules attach into a weakly-bound state based on this function, and so we approximate the η_1 distribution as a Gaussian function. For the strongly-bound cross-bridges, transition into this state occurs in the same manner, but detachment is force-dependent and favors smaller extensions, so we approximate the η_2 distribution with a Gaussian centered slightly to the right of 0. Throughout our approximation, we allow these means to vary when appropriate, but assume that their standard deviations are constant (this is equivalent to truncating our moment approximation).

Next, we implement a separation of time scales and solve the system on each interval. The force transient response suggests three time scales: 1) Pre-stretch: the muscle is activated and has reached steady-state, 2) Fast time: the stretch occurs at the start of this interval, all bound cross-bridges are stretched, and the fast weakly-bound cross-bridges re-adjust, and 3) Slow time: the weakly-bound cross-bridges are in steady-state and the strongly-bound cross-bridges slowly adjust back from the stretched position.

We solve each time scale individually below. In the following, we use G to denote normalized Gaussian functions with mean μ so that $\int_{-\infty}^{\infty} G(x,\mu)dx = 1$.

Pre-Stretch/Isometric: Pre-stretch the muscle has been activated and allowed enough time to reach steady-state. We approximate the pre-stretch η distributions as described above,

$$\eta_1 = \alpha_1(t)G_1(x,0) \tag{14}$$
$$\eta_2 = \alpha_2(t)G_2(x,\mu_2^a(t))$$

Using these approximations, we can transform our system in Eq. 13 into a system of ordinary

differential equations:

$$\frac{d\alpha_1}{dt} = k_{w_0}^+ N_5 - (k_w^- + k_a)\alpha_1$$

$$\frac{d\alpha_2}{dt} = k_a\alpha_1 - \alpha_2 \int_{-\infty}^{\infty} k_D(x)G_2(x, \mu_2^a(t))dx$$

(15)

$$\frac{d\mu_2^a}{dt} = \frac{-\sigma^2\left[\mu_2^a\left(k_a\alpha_1 - \alpha_2 \int_{-\infty}^{\infty} k_D(x)G_2(x, \mu_2^a)dx\right) + \alpha_2 \int_{-\infty}^{\infty} xk_D(x)G_2(x, \mu_2^a)dx\right]}{\alpha_2\left(\int_{-\infty}^{\infty} x^2 G_2(x, \mu_2^a)dx - (\mu_2^a)^2\right)}$$

$$\frac{dN_5}{dt} = k_w^-\alpha_1 + k_h^+(1 - \alpha_1 - \alpha_2 - N_5) - (k_h^- + k_{w_0}^+)N_5$$

For the purposes of our calculation, we are only interested in the pre-stretch steady-state force. We solve the above system under steady-state conditions by implementing a non-linear root find and using Matlab's `fsolve` function. This gives steady-state values for α_1^{ss}, α_2^{ss}, $\mu_2^{a,ss}$ and N_5^{ss}. Finally Eq. 2 can be used to calculate pre-stretch isometric force.

Fast Time: We assume that the stretch occurs at the start of this time scale. This means that the steady-state distributions of η_1 and η_2 are shifted by the amplitude of the stretch imposed, s. Throughout this fast time scale, the weakly-bound cross-bridges adjust back to steady-state, so the η_1 distribution adjusts from the stretched position back to be centered at 0. The strongly-bound cross-bridges act on a much slower time scale, and so we assume they are constant and are well-approximated by the Gaussian in the shifted position.

Under these conditions, our distributions become:

$$\eta_1 = A(t)G_1(x, \mu_1^b(t)) + (\alpha_1^{ss} - A(t))G_1(x, 0) \tag{16}$$
$$\eta_2 = \alpha_2^{ss}G_2(x, \mu_2^B)$$

with $A(0) = \alpha_1^{ss}$, $\mu_1^b(0) = s$, $\mu_2^B = \mu_2^{a,ss} + s$. Note that here, α_1^{ss}, α_2^{ss}, and $\mu_2^{a,ss}$ are the respective steady-state values from the previous solution for pre-stretch conditions.

On this fast time scale, we additionally assume that N_5 is in steady-state. This allows us to solve the system, and using the initial condition that $\eta_1(x, 0) = \alpha_1^{ss}G_1(x, s)$, we get an expression for η_1,

$$\eta_1 = \alpha_1^{ss}G_1(x, s)e^{-(k_w^- + k_a)t} + \frac{k_w^+(x)N_5^{ss}}{k_w^- + k_a}\left(1 - e^{-(k_w^- + k_a)t}\right) \tag{17}$$

And finally, we can again use Eq. 2 to solve for $F(t)$ on this time scale.

Slow Time: On the final time scale, we assume that the weakly-bound cross-bridges have re-adjusted, and now the strongly-bound cross-bridges are adjusting from the stretched distribution

back to steady-state. Thus, the η_1 distribution stays centered near 0, and the η_2 distribution begins in a shifted position and adjusts back to be centered near 0, as follows:

$$\eta_1 = a_1(t)G_1(x,0) \tag{18}$$

$$\eta_2 = a_2(t)G_2(x,\mu_2^a(t)) + b_2(t)G_2(x,\mu_2^b(t))$$

with $a_1(0) = \alpha_1^{ss}$, $a_2(0) = 0$, $b_2(0) = \alpha_2^{ss}$, $\mu_2^a(0) = 0$, and $\mu_2^b(0) = \mu_2^{a,ss} + s$. Again, note that steady-state values refer to pre-stretch steady-state.

To solve this, we must assume that $\mu_2^a << \mu_2^b$, i.e. that the means of the two Gaussians for the stretched and un-stretched positions are far apart. This allows us to assume that there are neighborhoods around both μ_2^a and μ_2^b where they are separate, and can therefore be integrated independently.

We use these approximations in Eq. 18 to transform the system of PDEs in 13 into the following set of ODEs:

$$\frac{da_1}{dt} = k_{w0}^+ N_5 - (k_w^- + k_a)a_1$$

$$\frac{da_2}{dt} = k_a a_1 - a_2 \int_{-\infty}^{\infty} k_D(x)G_2(x,\mu_2^a)dx$$

$$\frac{db_2}{dt} = -b_2 \int_{-\infty}^{\infty} k_D(x)G_2(x,\mu_2^b)dx$$

$$\tag{19}$$

$$\frac{d\mu_2^a}{dt} = \frac{-\sigma^2\left[\mu_2^a(t)\left(k_a a_1 - a_2\int_{-\infty}^{\infty} k_D(x)G_2(x,\mu_2^a)dx\right) + a_2\int_{-\infty}^{\infty} xk_D(x)G_2(x,\mu_2^a)dx\right]}{a_2\left[\int_{-\infty}^{\infty} x^2 G_2(x,\mu_2^a)dx - (\mu_2^a)^2\right]}$$

$$\frac{d\mu_2^b}{dt} = \frac{-\sigma^2\left[-\mu_2^b\int_{-\infty}^{\infty} k_D(x)G_2(x,\mu_2^b)dx + \int_{-\infty}^{\infty} xk_D(x)G_2(x,\mu_2^b)dx\right]}{\int_{-\infty}^{\infty} x^2 G_2(x,\mu_2^b)dx - (\mu_2^b)^2}$$

$$\frac{dN_5}{dt} = k_w^- a_1 + k_h^+(1 - a_1 - a_2 - b_2 - N_5) - (k_h^- + k_{w0}^+)N_5$$

This system of ODEs is much faster to solve numerically than our original system of PDEs.

Thus, with the above approximation, we have separated the force transient behavior into three time scales, approximated the system of PDEs with a system of ODEs, solved numerically, and calculated the resulting force. In total, we have an efficient method for approximating $F(t)$. Additionally, we find that this approximate solution is very close to the more accurate full numerical solution

(Fig. S2). Thus, this approximation is advantageous because it can be used to preliminarily fit force transient measurements, resulting in a very good approximation of best-fit parameters, which can then be used as an initial condition to optimizing the more accurate full RK4 numerical solution.
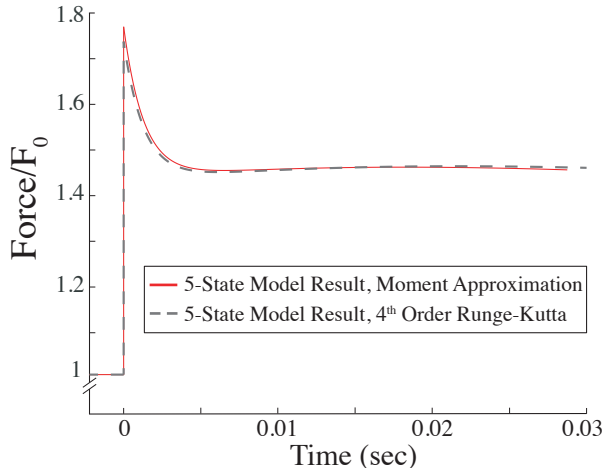
Figure S2: Model simulation of a force transient response to a quick stretch: The model can be solved numerically using fourth-order Runge-Kutta (see section 1.4.1) to provide an accurate result for force as a function of time (gray, dotted line). For efficiency, the model can additionally be approximated using separation of time scales and a modified moment approximation (see section 1.4.2), resulting in a method of solving the system that is both a very good approximation to the numerical solution (red, solid line), and efficient enough to perform preliminary parameter optimizations.

2   Four-State Model + Viscous Drag

2.1   Weak Binding Acts as a Viscous Drag

In the motivation section of the main text, we begin by introducing a four-state model (Fig. 1A of main text) which has been previously shown to describe molecular muscle measurements and force-velocity measurements from muscle fibers [1, 6]. Based on experimental evidence [7, 8, 9, 10, 11, 12], we hypothesize that this model must additionally include a weakly-bound interaction between actin and myosin, leading to the five-state model (Fig. S1 and Fig. 1B of the main text). Given that weakly-bound myosin molecules rapidly bind and unbind from the actin filament without undergoing a power-stroke [8, 10], and given that the rate constants for weak binding (k_w^- and k_a) do not depend on force, these cross-bridges act as a viscous drag on the system [13] (Fig. S3). This provides us with another method of efficiently approximating the five-state model in force-velocity measurements: we can add a viscous drag to the four-state model.

We initially use this method to fit the force-velocity data of A. V. Hill and the energetics data of W. O. Fenn, and to motivate the necessity of a weakly-bound state in the main text. To do so, we solve the four-state model to get force as a function of shortening velocity, and then subtract a linear function from this result. The slope of this line determines the amount of viscous drag, or equivalently, the amount of weakly-bound cross-bridges. With this force-velocity relationship, we

can also calculate total energy as a function of force. We find that the four-state model with viscous drag is able to simultaneously fit Hill's force-velocity and Fenn's energetics data, motivating our hypothesis that weak binding is necessary to consistently model muscle measurements.

2.2 Parameter Optimization and the Four-State Model

In addition to motivating our hypothesis, we used the four-state model with drag to identify parameters that can describe our own force-velocity measurements (Figs. 2D, 3B and 4B of the main text) because it has fewer parameters and is more computationally efficient than the five-state model. The parameter combinations for the four-state model with drag were identified by fixing a particular amount of drag (i.e. amount of weakly-bound cross-bridges), and performing an optimization to determine the best fit ADP release rate (k_D^0) and force-dependent parameter (E). We use a matched asymptotic analytical solution to the four-state model to get close to the best-fit parameters, and then perform the final optimization using a numerical solution to the four-state model. We optimize using Matlab's `fminsearch`, and define the error as the sum of the squared difference between the model and measurements divided by the number of data points. In the four-state model at steady-state, E and k_D^0 are the only two unknown parameters. Our results are plotted as gray squares in Fig. S4a.

This parameter optimization is much simpler than the equivalent optimization with the five-state model, which includes three additional unknown parameters (k_w^-, k_a, and $k_{w_0}^+$), which determine the time scale and amount of weak binding. In fact, the combinations of E and k_D^0 that fit the five-state model to force-velocity measurements are not unique, but are dependent on the time scale of weak-binding. Thus, to fit the five-state model, we must fix one of the weak-binding parameters (either k_w^- or k_a), which specified the time scale of weak binding, and then fit the other unknown parameters. By fixing E at different values, we get combinations of E and k_D^0 that result in good fits of the five-state model to the force-velocity measurements (colored symbols in Fig. S4a).

These fits demonstrate two important results. First, we find that as the time scale of weak binding
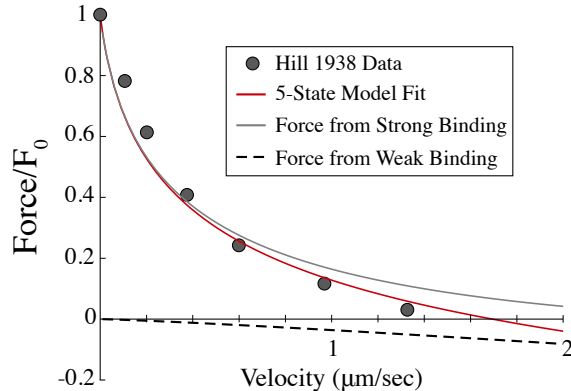
Figure S3: Weakly-bound cross-bridges act as a viscous drag. The five-state model fits force-velocity measurements (red line, data from [14]). This total force is comprised of the force from strongly-bound cross-bridges (gray, solid line) and force from weakly-bound cross-bridges (black, dotted line). The linear relationship between force and velocity generated by the weakly-bound cross-bridges demonstrates that they act as a viscous drag on the system.

increases, the five-state model results approach those of the four-state plus drag (Fig. S4). Second, when we violate the assumption that weak binding is fast compared to strong binding, the four-state model plus drag underestimates the ADP release rate necessary to fit our measurements, i.e. the k_D^0 values predicted from the the four-state model plus drag are a lower bound to those predicted by the five-state model. This latter fact is useful when we compare the five-state model fits to our force-velocity and force transient measurements. Because the best-fit k_D^0 value at a given E for the force transient measurements are always less than the equivalent k_D^0 value for our force-velocity measurements, the five-state model force-velocity fits will give parameters equivalent to, or worse than, those from the four-state plus drag. Therefore, for simplicity, we use the four-state plus drag force-velocity parameters (Figs. 2D, 3B, and 4B of the main text) to compare to force transient results.
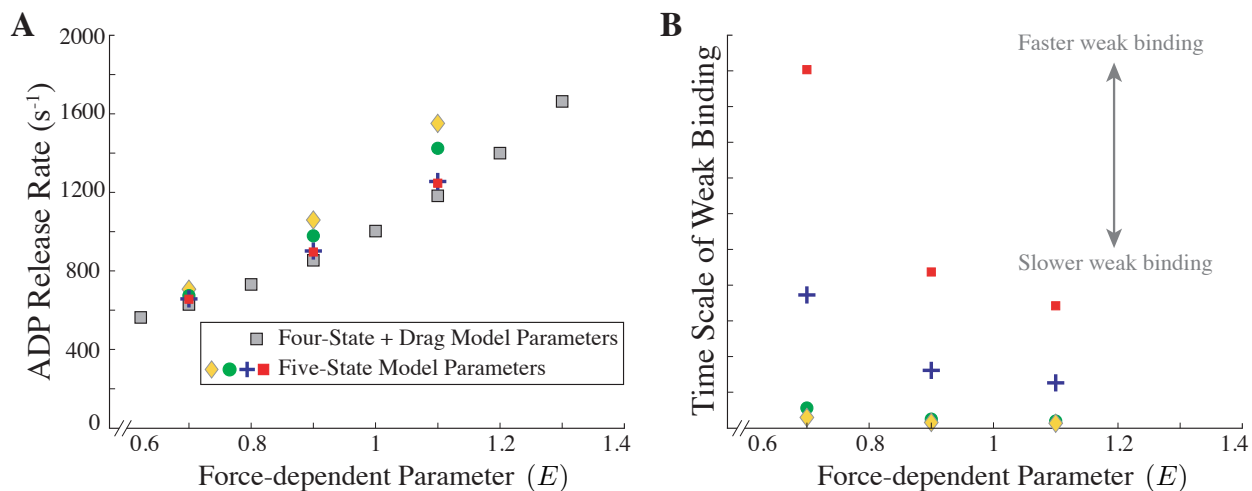
Figure S4: As the time scale of weak-binding increases, the five-state model approaches the four-state model plus drag. **A:** Best-fit combinations of unloaded ADP release rate (k_D^0) and the force-dependent parameter (E) for the four-state model plus various amounts of drag (gray squares) and the five-state model with various weak-binding time scales (colored symbols). For each colored symbol, one of the weak binding parameters (k_w^- or k_a) was fixed along with the force-dependent parameter (E), and the other parameters were optimized. The four-state model parameters are a lower bound to the five-state results. **B:** This panel illustrates the weak-binding time scale corresponding to each colored symbol in panel A. As the time scale of weak binding increases, the five-state predictions in panel A approach those of the four-state model.

3 Weak Binding is Necessary for Consistent Force-Dependence: Modeling Classic Measurements of the Energetics of Muscle (Fenn 1923) and the Force-Velocity Relationship (Hill 1938)

In the main text, we motivate the necessity of a weakly-bound state in modeling the interaction between actin and myosin by fitting the four- and five-state models to classic measurements from W.O. Fenn (1923) and A.V. Hill (1938). Here, we discuss how we model these measurements, the details of the optimization, and the statistical significance of our results.

3.1 Modeling the Energetics of Muscle

In his work, W.O. Fenn measured energy liberation during muscle contraction. Experimentally, a muscle was maximally stimulated for a fixed time and allowed to shorten a fixed distance. Fenn measured the work done by the muscle and the heat produced as a function of the load imposed [15].

To model this relationship, we first note that due to conservation of energy, total energy is equal to work done plus heat released. In our case, ATP hydrolysis fuels the cyclical interaction between actin and myosin, so total energy is equivalent to the energy of ATP hydrolysis, which we call E_{ATP}. One molecule of ATP is hydrolyzed each time a myosin molecule completes the actomyosin cycle. Thus, the flux through an irreversible step of the cycle gives the rate of ATP consumption, which is proportional to the time derivative of E_{ATP} (the proportionality constant is the energy of ATP hydrolysis). We integrate this expression to get $E_{ATP}(v)$ where v is velocity. Additionally using our calculated force-velocity relationship, we have an expression for total energy as a function of force, which directly relates to Fenn's measurements.

Implementing the above with the five-state model, we find that weak binding has a minimal effect on this calculation. With the addition of weakly-bound cross-bridges, the muscle must do more work to overcome the resistive force of these cross-bridges. However, we find that the magnitude of this work is small compared to the work necessary for the muscle to raise the weight (Fig. S5). Additionally, the magnitude of the overall work is small compared to the heat produced by the muscle. In Fenn's original measurements, the heat produced was an order of magnitude larger than the work done by the muscle [15].
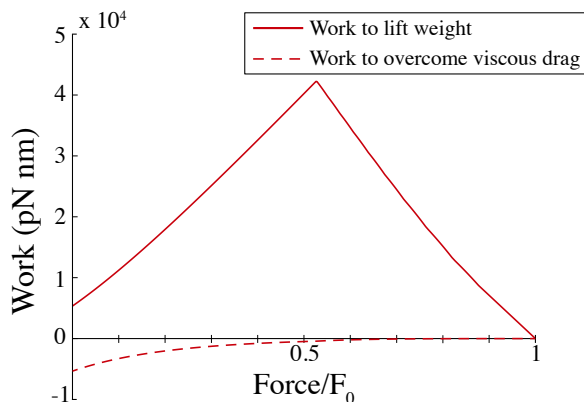
Figure S5: Weak binding has a minimal effect on work done by a muscle. Simulating Fenn's experimental protocol using the five-state model results in work done by the muscle to lift the weight (red solid line) that is much larger than the work done to overcome resistive force from weakly-bound cross-bridges (dotted red line).

3.2 Fitting Model to Energetics and Force-Velocity Data

To compare the model to Hill's force-velocity and Fenn's energetics data, we first solve for the model's force-velocity relationship (see section 1). This is directly comparable to Hill's measurements. Next, based on the above calculation, we solve for total energy as a function of force, which

is comparable to Fenn's measurements.

We fit the four- and five-state models to the data [14, 15]. In the case of the energetics data, we multiply the normalized force data by 0.9. This gives a better fit between model and data, and we justify it by the fact that true isometric force of a muscle is extremely challenging to measure and is not directly reported in Fenn's paper. We perform fits to the data by simulating the model for a given parameter set, calculating the error as the sum of the squared difference between model and data divided by the number of data points, and optimizing using Matlab's `fminsearch`. When simultaneously fitting energetics and force-velocity data, we define the error as the sum of the individual errors, with the force-velocity error weighted slightly higher.

Because the four- and five-state models have two and four unknown parameters respectively, we tested whether the five-state model was a better fit with an F-test, which yields $p < 0.05$. We therefore conclude the five-state model gives a significantly better fit than the four-state. Additionally, we find that the five-state model fits are insensitive to one of the unknown parameters. Thus, if the five-state model differs from the four-state model by only one extra parameter, the difference between the two models is more significant.

4 Mismatch Between Force Transient Data and Model is not Unique to *Drosophila* Jump Muscle

In section 3.1 of the main text, we describe a discrepancy between our model predictions and our force transient measurements. In particular, our model predicts a peak force post-stretch (phase I) that is at least twice what we measure in *Drosophila* jump muscle. Importantly, the model prediction is a lower bound, since the calculation accounts only for force from strongly-bound cross-bridges that have undergone a power-stroke. Thus, if weakly-bound cross-bridges are also present, they will produce additional force once stretched, leading to an even larger discrepancy between model and measurements.

This difference is not unique to *Drosophila* jump muscle. In fact, measurements from a variety of vertebrates and a range of muscle fiber types result in peak forces that are similar to our measurements (Fig. S6, [16, 17, 18, 19]). While some of the experimental measurements are above our predicted line, the majority are not. Additionally, since the predicted line is a lower bound, measurements must be well above this prediction to be fit by the model. If the weakly-bound state is significantly populated, we would expect peak forces to be higher than the predicted lower bound by a factor of 2 or more. Thus, of the fifteen measurements considered here, only four have the potential to be fit by the model ([20, 21] and fiber types I and IIA from [22]).

5 Explanation 1: Overestimated Stretch Amplitude

In the main text, we discuss how our model, with the assumption of linear cross-bridge elasticity, is inconsistent with force transient measurements because the model predicts a peak force post-stretch that is significantly larger than that measured (Fig. 2B main text). In section 3.2, we
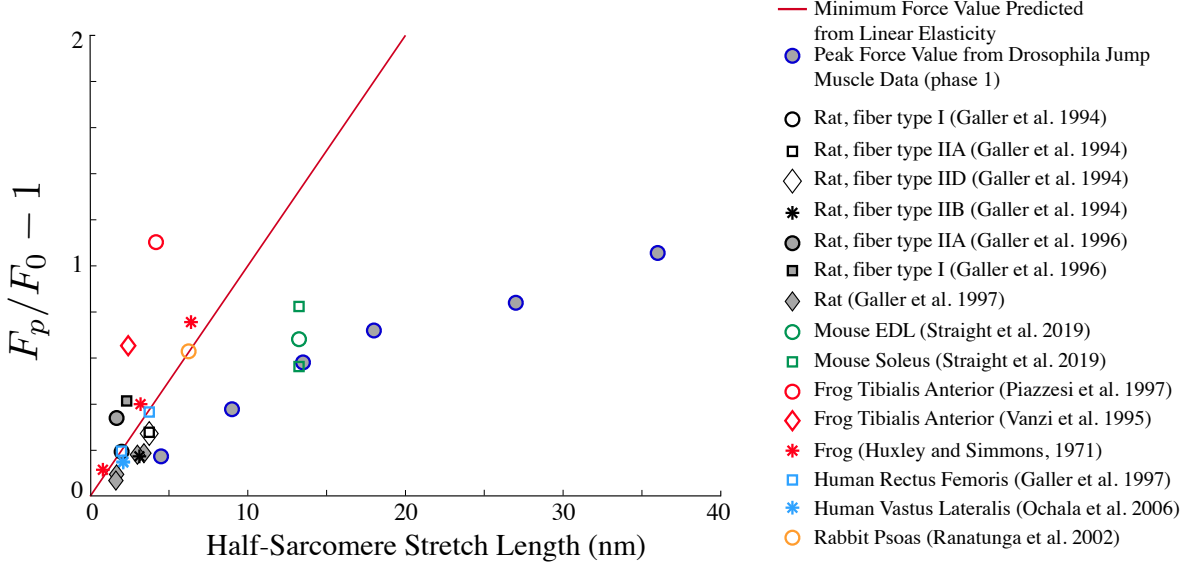
Figure S6: Peak force above isometric force in transient response after rapid stretch (phase I) as a function of stretch size. Measurements from a variety of muscle fiber types are at or below the model's prediction.

present an argument against the possibility that this discrepancy is caused by an overestimated stretch amplitude at the sarcomere level due to series elasticity. Here, we provide further details on the computation that led to this conclusion.

5.1 Fitting Model with Decreased Stretch Amplitude

To fit the model to force transient measurements for the case of overestimated stretch amplitude, we allow the unknown model parameters to vary (k_w^-, k_a, k_D^0, E), and additionally include the stretch amplitude, Δs, as an unknown parameter. Note that in the force transient measurements, the force does not return to steady-state for long time, but instead remains slightly higher than the pre-stretch isometric value. Our model does not account for this residual force enhancement. Thus, in order to compare the model to the data, we must shift the force transient measurements so that the force returns to steady-state. To simulate the force transient, we solve the system numerically using RK4. To compare the results to our measurements, we define error as the sum of the squared difference between the model results and the shifted data divided by the number of data points, and optimize using Matlab's `fminsearch`.

We fit the model to a force transient measurement with a stretch amplitude of 0.5% muscle length (main text Fig. 2A). Assuming there is no effect of series elasticity, this corresponds to a 9 nm stretch at the half-sarcomere level. Our optimization results in a set of best-fit parameters, including a single best-fit value for the reduced stretch amplitude of $\Delta s = 0.437$ nm. The corresponding model fit is illustrated in Fig. 3A of the main text.

To estimate the range of Δs values that result in good fits to the data, we assume that the best-fit parameters give a perfect fit, and calculate the error in this case. We define the maximum acceptable error as $\sqrt{2} \cdot E_b$, where E_b is the error from the best-fit parameters. This gives us an estimate of the standard deviation of the best fit, and provides a benchmark for when the model is

different from the data. We find that only a small range of significantly decreased stretch amplitudes ($\Delta s = 0.4 - 0.55$ nm) result in good fits to the force transient measurements (Fig. S7).
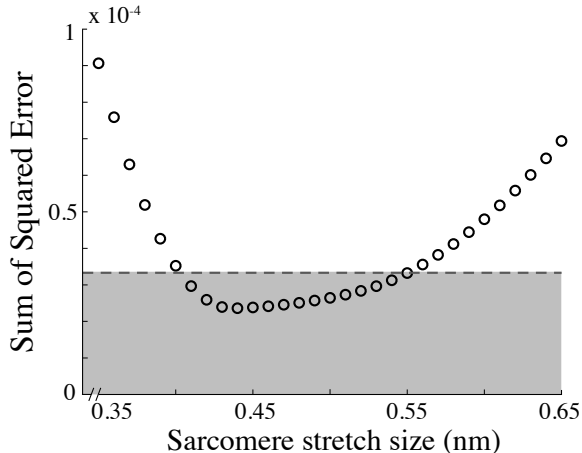
Figure S7: Sum of the squared error as a function of the half-sarcomere stretch size. For each point, the stretch amplitude was fixed and the other parameters were optimized to fit the model to a measurement from a 0.5% muscle length stretch. Values within the shaded region are considered acceptable fits, and represent error that is within one standard deviation of the error produced by the best-fit parameters.

## 5.2 Comparing Parameter Fits from Force Transient and Force-Velocity Measurements

Next, to compare the model fits of force transient measurements to fits of force-velocity measurements, we consider combinations of two model parameters, unloaded ADP release rate (k_D^0) and the force-dependent parameter (E) (Fig. 3B of the main text). To determine the force transient parameters, we perform the same fits as above, but with the stretch amplitude fixed at the best fit value of $\Delta s = 0.437$ nm. For the force-velocity parameters, we perform fits to the four-state model with various amounts of weak binding (see section 2.2 for justification). In each case, error is defined as the sum of the squared difference between model and data divided by the number of data points, and Matlab's `fminsearch` is used for optimization.

We determine the variability in these parameters by optimizing the model to determine the best-fit parameters at a given E, and use this result to define an upper bound on the acceptable error (see section 5.1). We sweep through k_D^0 values to determine a range that provides satisfactory fits to the data for the given E value. We perform this sensitivity analysis for both the force transient fits and the force-velocity fits (Fig. S8).

5.3 Explanation 1 Extended: Strong Binding Cannot Cause Phase I and II of Force Transient Response

In most of our analysis, we assume that phase I and II in the force transient response are attributed to weakly-bound cross-bridges that rapidly re-equilibrate post-stretch (Fig. 1F main text). However, it is also possible that the weakly-bound cross-bridges act on a faster time scale
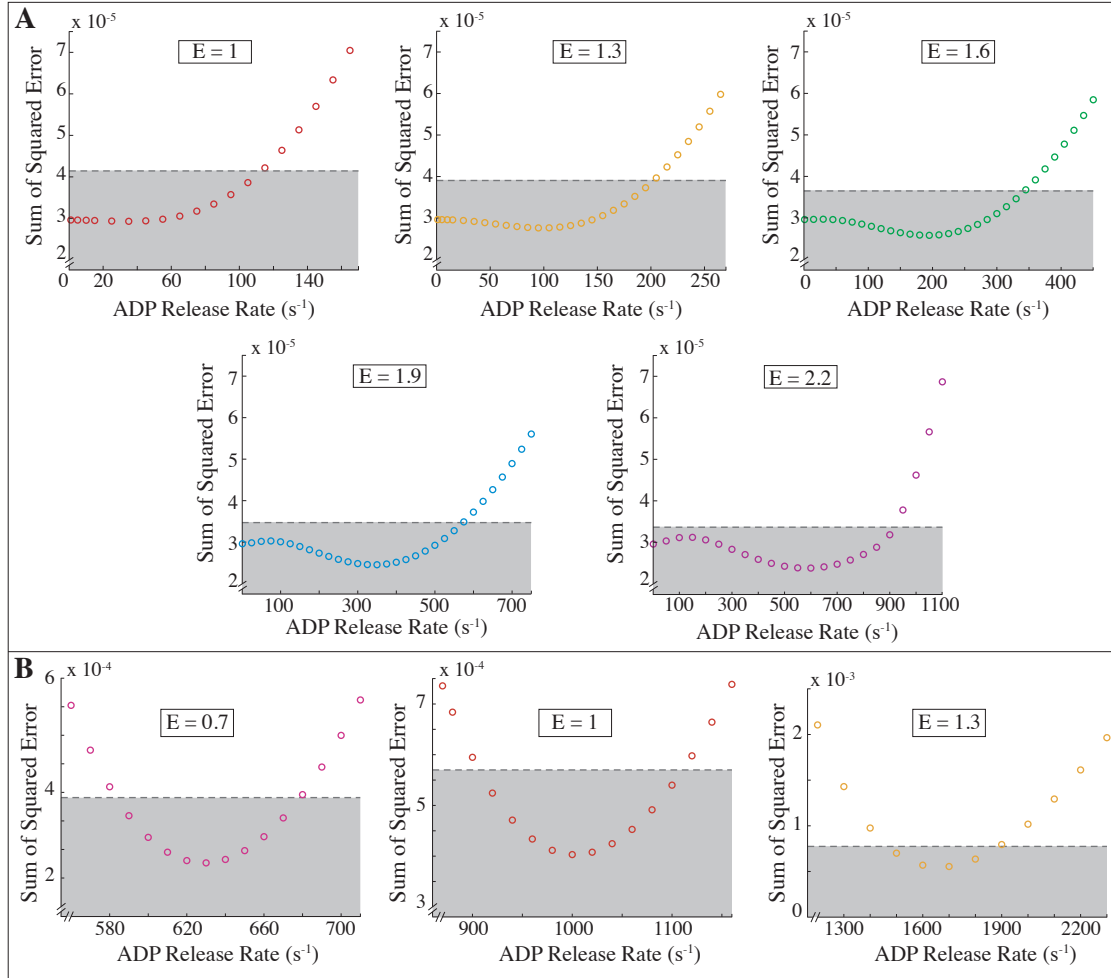
Figure S8: Sensitivity analysis for fitting model to data. In each, the gray shaded regions denote acceptable error, and represent error that is within one standard deviation from the error produced by each best-fit. These results are used to determine the error bars in Figs. 2D, 3B, and 4B of the main text. **A)** Sum of the squared error in fitting force transient measurements as a function of ADP release rate for a fixed force-dependence. For each panel, the five-state model (including Δs as an unknown parameter) is fit to the force transient measurement from a 0.5% muscle length stretch. **B)** Sum of the squared error in fitting force-velocity measurements as a function of ADP release rate for fixed force-dependence. For each panel, the four-state model plus drag was fit to force-velocity measurements.

than the temporal resolution of the force transient measurements (i.e. the time between data points, $\Delta t = 0.125$ ms). In this case, weakly-bound cross-bridges re-equilibrate before the first measurement post-stretch, and phase I and II of the force transient response are solely due to strongly-bound cross-bridges. Then, phase III and IV would arise from some other mechanism that is not included in our model.

To test our assumption that phase I and II are due to weakly-bound cross-bridges, we tested the viability of the model as described above, with weakly-bound cross-bridges acting on a time scale faster that the resolution of the measurements. To do so, we implemented two fourth-order Runge-Kutta algorithms to solve for force as a function of time. The first begins at the instant of stretch and iterates through time using a small time step ($\Delta t = 0.00625$ ms) until it reaches the first point

in time post-stretch from our measurements, $t = 0.125$ ms. The second RK4 algorithm begins at this time point and iterates through time using a larger step size ($\Delta t = 0.05$ ms). In this way, we can capture the rapid response of the weak-binding cross-bridges without having to maintain a short, and computationally inefficient, time step. We fix two of the weak binding parameters (k_w^- and $k_{w_0}^+$) to be large enough so that the weakly-bound cross-bridges have re-equilibrated by the end of our first RK4 simulation. We can then compare the result of the second RK4 simulation with our force transient measurement, ensuring that the peak is solely due to strongly-bound cross-bridges.
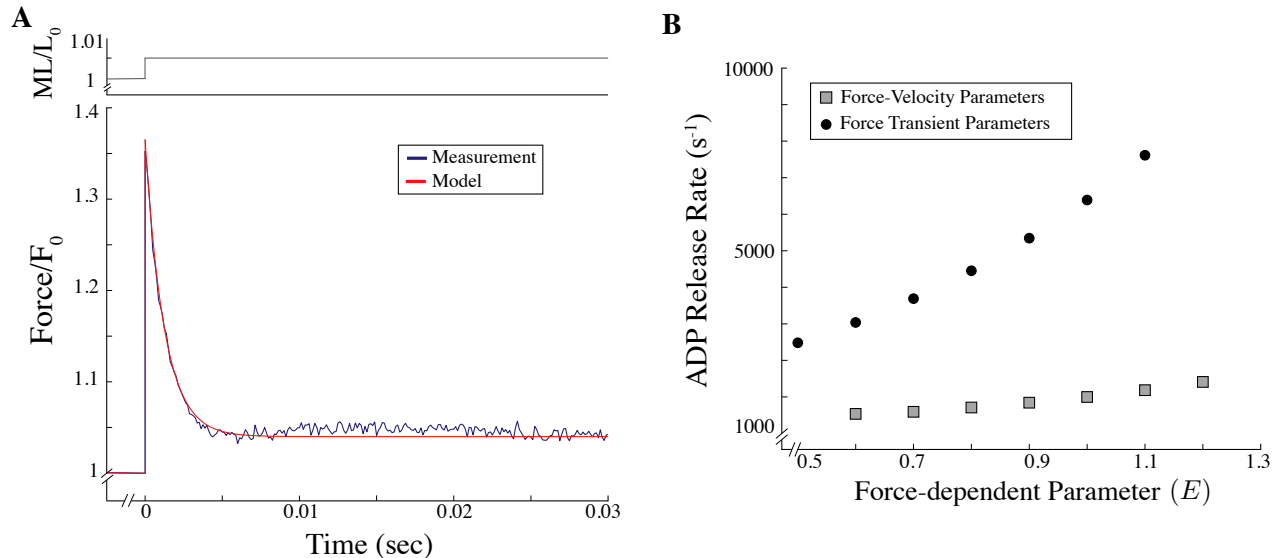
Figure S9: The model cannot simultaneously fit the force transient and force-velocity measurements with the assumption that the peak in force post-stretch is solely attributable to strongly-bound cross-bridges. **A)** Assuming strong-binding causes the peak in force post-stretch, the five-state model can fit the derivative of the force transient trace for a 0.5% muscle length stretch. The corresponding force trace is reproduced here. The model result has been shifted to account for an offset in the result due to fitting the derivative. The best-fit parameters suggest a decreased stretch amplitude ($\Delta s = 3.61$) and a negligible force-dependence ($E = 0.01$). **B)** Combinations of unloaded ADP release rate and the force-dependent parameter that fit the force transient measurements under these conditions (black circles) are inconsistent with those required to fit force-velocity measurements (gray squares). To fit model to data, the weak binding parameters k_w^- and $k_{w_0}^+$ were fixed to be large, and the five-state model was fit to both the force-velocity and force transient measurements.

As with our other models, this model is inconsistent with the measured peak force from our force transient traces (main text Fig. 2B). We must therefore adjust for this discrepancy, and we do so by letting the stretch amplitude be a parameter of fit (see section 3.2 of the main text for justification). Additionally, because phase III and IV of the force transient response would not be described by this model, we fit the derivative of the force transient trace. The advantage of this approach is that the derivative is invariant to the addition of a constant value being added to the force trace. Since phase III and IV act on a longer time scale that phase I and II, they are reasonably well approximated by a constant in this model.

With these assumptions and with this implementation, the model is able to fit our force transient measurements (Fig. S9a). However, it requires a small force-dependence and large unloaded ADP release rate (best-fit gives $E = 0.01$ and $k_D^0 = 830.07$ s^{-1}) to be able to reproduce the timescale of phase I and II. As we fix E and optimize the fit to the data, we find that the predicted ADP

release rate is too large to be consistent with the fits to our force-velocity measurements (Fig. S9b). Thus, phase I and II are too fast to be due to strongly-bound cross-bridges, and we conclude that the peak force cannot be attributed to detachment of strongly bound cross-bridges in this manner.

6   Explanation 2: Unexplained Force

In section 3.3 of the main text, we briefly present an argument against the presence of an additional force, not due to actin and myosin, in the force transient measurements. Here, we discuss our methods (sections 6.1, 6.2, 6.3, 6.4) and findings (section 6.5) in more detail.

6.1   Passive Force in Force Transient Measurements

When we consider that the force transient measurements may include additional non-cross-bridge forces, one possibility is that passive elements in the muscle fiber are contributing to the measured force. Our model only accounts for force from cross-bridge interactions, and therefore would not reproduce passive force.

To control for this, we perform the force transient measurements at low calcium concentrations (pCa 8.0). At this low calcium concentration, there is very little cross-bridge cycling, and thus any force produced can be attributed to passive elements. We find that the force produced for pCa 8.0 is negligible compared to that produced at a saturating calcium concentration of pCa 5.0 (Fig. S10a, b). In particular, we find that the pre-stretch isometric stress value for pCa 5.0 is 15 - 20 times greater than the pre-stretch isometric stress value for pCa 8.0 (Fig. S10c). Notably, this difference in magnitude is present for all of the fibers and at every stretch amplitude we considered, confirming that the force from passive elements is negligible across all of our experimental conditions.
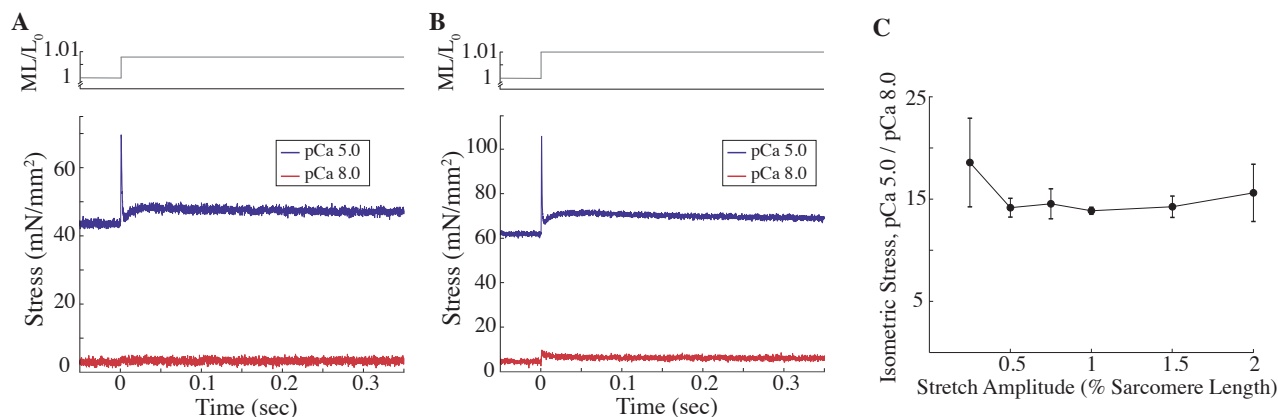
Figure S10: Passive stress produced for pCa 8.0 is negligible compared to active stress produced at pCa 5.0. **A**, **B**: Stress (mN/mm^2) as a function of time (sec) for muscle fibers quickly stretched a small percentage of their length (A: 0.75% ML, B: 1% ML) at saturating calcium concentration of pCa 5.0 (blue) and low calcium concentration of pCa 8.0 (red). **C**: Ratio of pre-stretch isometric stress at pCa 5.0 compared to that at pCa 8.0 at various stretch amplitudes. Each data point includes values from two fibers. Together, these plots illustrate that the passive force produced at low calcium concentrations is negligible, and about 15 times less than that produced at saturating concentrations.

19

6.2 Adjusting Model to Include Non-Cross-Bridge Force

While the above experiments show that purely passive elements are not contributing significantly to force, there is evidence that some elastic elements in muscle stiffen in the presence of calcium [23] or that non-cross-bridge elements can contribute to force [24]. It is possible, then, that the contribution of these elements to muscle force underlie the discrepancy between our measurement of peak force, and that predicted by Eq. 1 of the main text, reproduced below:

$$\frac{F_p}{F_0} = \frac{(\mathcal{S}+d)\kappa}{d\kappa} = \frac{\mathcal{S}}{d} + 1 = \frac{1800 \cdot s\%}{d} + 1 \tag{20}$$

where κ is myosin's stiffness, d is myosin's step size, F_p is peak force post-stretch, F_0 is pre-stretch isometric force, and $\mathcal{S}$ is stretch length:

We call the force produced by these non-cross-bridge elements an "unexplained force". To account for this, we let it be a parameter in the model. Additionally, we let this value be different pre- and post-stretch. Thus, the force calculation in Eq. 20 becomes,

$$\frac{F_p}{F_0} = \frac{F_{xb}^p + F_{nc}^p}{F_{xb}^0 + F_{nc}^0} \tag{21}$$

where F_{xb}^0 and F_{xb}^p are the cross-bridge forces pre- and post-stretch, and F_{nc}^0 and F_{nc}^p are the non-cross-bridge forces pre- and post-stretch, respectively. While this initially introduces two new parameters to the model, we can use the following calculation to reduce it to just one new parameter.

The model predicts that for long time after stretch, the force from cross-bridges will be equal to the pre-stretch cross-bridge isometric force. In the force transient data, however, the post-stretch steady-state value is slightly higher than the pre-stretch value. We must account for this residual force enhancement [25], which would not be reproduced by these models [26] and would therefore lead to inaccurate parameter estimation. We account for this, and reduce the number of parameters-of-fit, with the following calculation, where F^* denotes the post-stretch steady-state value normalized to the pre-stretch steady-state in the data:

$$\lim_{t \to \infty} \frac{F_p}{F_0} = \frac{F_{xb}^0 + F_{nc}^p}{F_{xb}^0 + F_{nc}^0} = F^* \tag{22}$$

The force transient measurements determine the F^* value, and thus we can solve for F_{nc}^p in terms of F_{nc}^0. Thus, to account for this non-cross-bridge force, we fit the force transient measurements to,

$$\frac{F_p}{F_0} = \frac{F_{xb}^p + F^*(F_{nc}^0 + F_{xb}^0) - F_{xb}^0}{F_{xb}^0 + F_{nc}^0} \tag{23}$$

where the cross-bridges forces are determined from the five-state model and F_{nc}^0 is an additional parameter of fit that determines the amount of unexplained force due to non-cross-bridge effects.

6.3 Fitting Model with Unexplained Force

To fit the model to the force transient measurements for the case of unexplained force, we allow the unknown model parameters to vary (which now includes the parameter for additional unexplained

force, F_{nc}^0). Note that in this case, we fix the stretch amplitude to be at the true experimental value. We use RK4 to solve the system for force as a function of time, define error as the sum of the squared difference between model and data divided by the number of data points, and use Matlab's `fminsearch` to optimize the parameters.

The optimization results in a set of best-fit parameters, including a best-fit value for F_{nc}^0. To determine the range of F_{nc}^0 values that can result in good fits to the data, we bound the error by $\sqrt{2} \cdot E_b$, where E_b is the best-fit error (see section 5.1). We find that only a small range of values for F_{nc}^0 result in acceptable errors (Fig. S11a).

Additionally, to consider the plausibility of these results, we compared the unexplained force values, F_{nc}^0, to the isometric force from cross-bridges, F_{xb}^0 (Fig. S11b). Note that the isometric cross-bridge force changes for different amounts of unexplained force. Thus, normalizing F_{nc}^0 by F_{xb}^0 results in multiple error values for the same ratio of unexplained force to cross-bridge force (Fig. S11b). However, there is a clear minimum and a single error value for each choice of unexplained force (Fig. S11a). This best-fit unexplained force is 28.07 times that of isometric force from cross-bridges, and that parameters that result in acceptable error predict an unexplained force that is 27 - 28.3 times that of isometric. We conclude that it is unreasonable to expect that force transient measurements include an unexplained force of this magnitude.
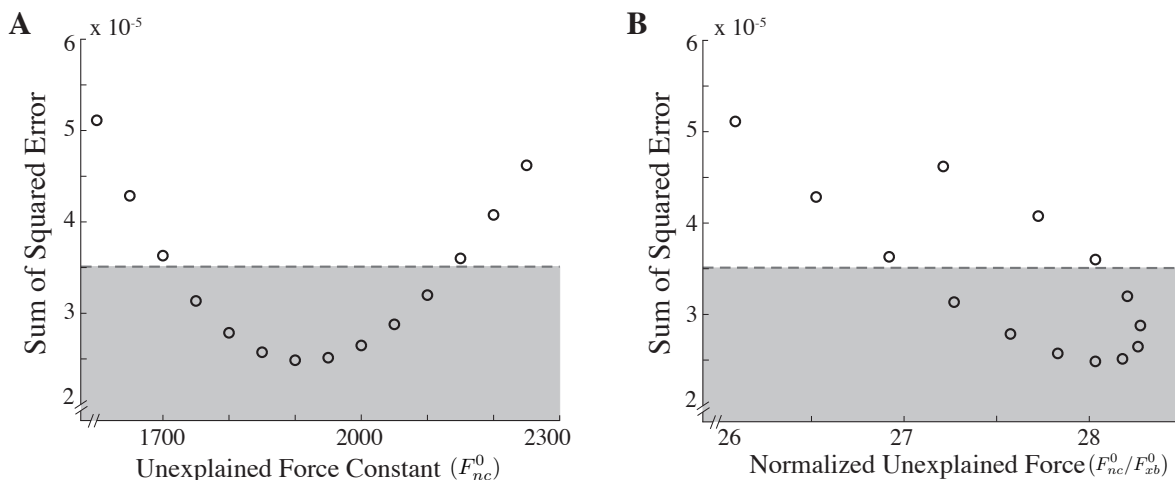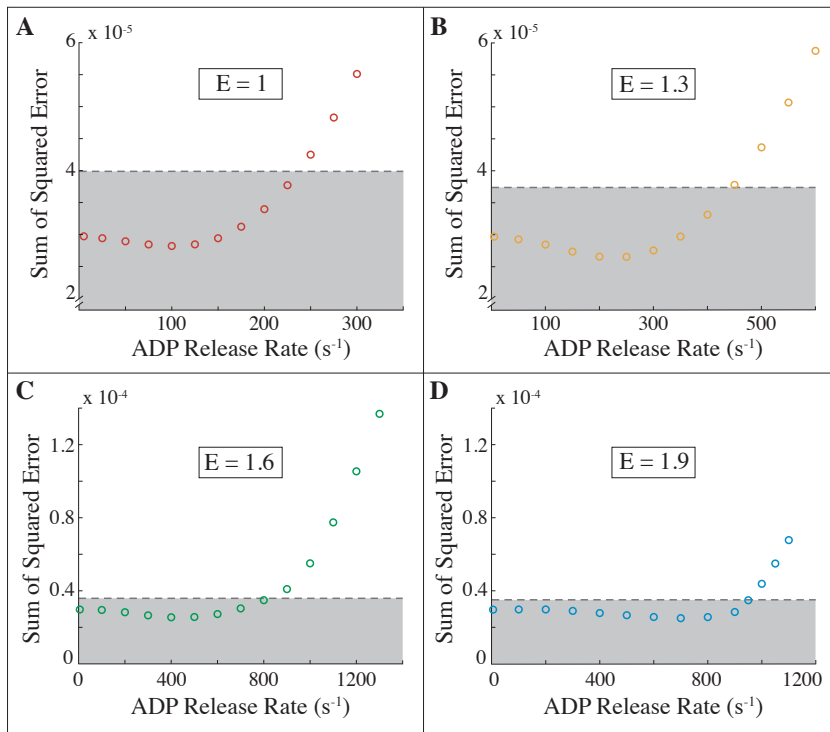

Figure S11: Sum of the squared error as a function of: **A)** the unexplained force value, F_{nc}^0, and **B)** the unexplained force value normalized to pre-stretch isometric cross-bridge force, F_{nc}^0/F_{xb}^0. For each point, the F_{nc}^0 value was fixed, and the five-state model was fit to the force transient measurement. Values of F_{nc}^0 that result in acceptable error lie in the shaded box, which denotes error that is within one standard deviation of the best fit. The best-fit values suggest that the non-cross-bridge forces are around 28 times that of isometric cross-bridge force.

6.4 Comparing Parameter Fits from Force Transient and Force-Velocity Measurements

We also compared the force transient fits to the force-velocity fits under these conditions. For the force transient measurements, we let the unknown parameters (including F_{nc}^0) vary, and determine the best-fit combinations of ADP release rate and force-dependence. The force-velocity parameters

are based on the four-state plus drag fits (see section 2.2 for justification). In both cases, error is defined as the sum of the squared difference between model and data divided by the number of data points, and Matlab's `fminsearch` is implemented for optimization. Additionally, we perform a sensitivity analysis (see section 5.1) to consider the variability in acceptable parameters due to noise in the data (Fig. S12).


Figure S12: Sum of the squared error in fitting force transient measurements as a function of ADP release rate for a fixed force-dependence. For each panel, the five-state model (including F_{nc}^0 as an unknown parameter) is fit to the force transient measurement from a 0.5% muscle length stretch. The gray shaded regions denote acceptable error, and represent error that is within one standard deviation from the error produced by each best-fit. This sensitivity analysis leads to the error bars on the force transient measurements in Fig. S13b.

6.5 Rejection of Unexplained Force as Explanation for Model and Measurement Discrepancy

Comparing the five-state model with an unexplained force to our force transient measurements, we find that the optimization converges to a good fit to the entire force transient measurement, reproducing all parts of the force response (i.e., phases I-IV, Fig. S13a). However, we reject this explanation for two reasons. The first is that the best-fit predicts an implausibly large unexplained force of about 28 times that of the isometric force from cross-bridges (Fig. S11b).

The second reason we reject unexplained force as the source of the discrepancy between simulation and measurement is that the force-dependence required for the force transient fits is inconsistent with the force-dependence required for the force-velocity fits (Fig. S13b). In particular, the force transients require a large force-dependence that results in a force-velocity relationship that is too
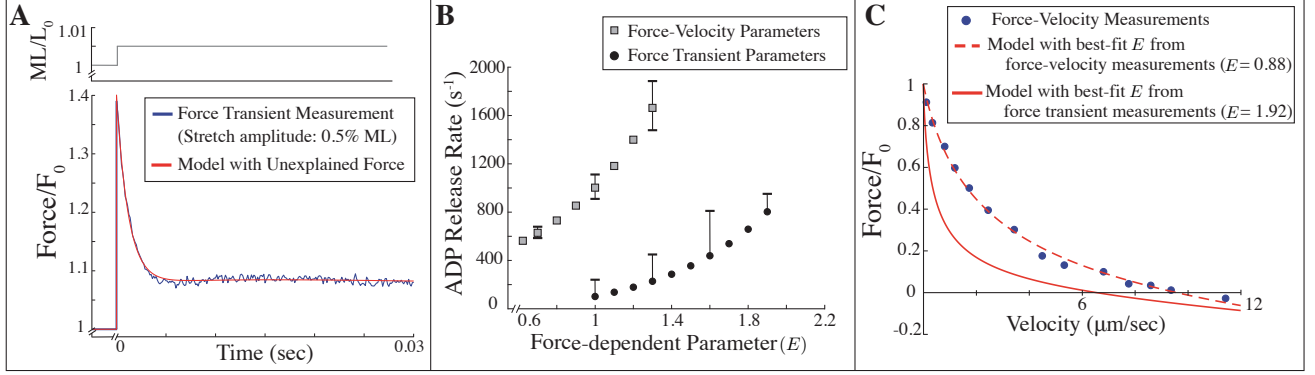
Figure S13: The model reproduces the force transient measurements given the addition of a non-cross-bridge force, but the results are inconsistent with force-velocity measurements. **A)** Including an unexplained force in the force response that is 28.1 times that of isometric cross-bridge force allows the five-state model to fit force transient measurements. **B)** Combinations of unloaded ADP release rate and the force-dependent parameter that fit force-velocity (gray squares) and force transient (black circles) measurements when the force transient includes a non-cross-bridge force. Error bars denote parameter values that give results within one standard deviation of the best-fit error. **C)** Model fits to force-velocity measurements with k_D^0 fixed from the best-fit to the force transient measurement, and E from the best-fit to the force transient measurement (sold line) and best-fit to the force-velocity measurements (dashed line).

curved (Fig. S13c). This result is similar to our fits with decreased stretch amplitude due to series elasticity (main text Fig. 3B). In that case, the model required an increased force-dependence (i.e. larger E) to counteract the decreased stretch amplitude and to produce phase III of the force transient response (see main text, section 3.2). However, in the case of unexplained force, our fits have the full stretch amplitude, so we expected to see a leftward shift (toward smaller values of E) in the best-fit parameters for our force transient measurements, and therefore better agreement with the best-fit parameters for our force-velocity measurements. Indeed, we observed such a shift (compare main text Fig. 3B to Fig. S13b), but it is modest and insufficient to allow us to find a single parameter set to fit both of our measurements.

These fits still require a large force-dependence because of the large magnitude of the unexplained force. In the normalized force transient response, the amplitude of force increases (phase I and III) is measured relative to the total isometric force. Thus, if isometric cross-bridge force makes up less of the total isometric force, the amplitude of phases I and III relative to the isometric cross-bridge force increases. For example, we measured a peak force (phase I) of ~ 1.4 times isometric, which is $\sim 40\%$ above isometric force (main text Fig. 2A). If all force arises from cross-bridges, then this peak force results in a $\sim 40\%$ increase in cross-bridge force. However, suppose that isometric force is half due to cross-bridges and half due to an unexplained force. In this case, the increase in force due to cross-bridges will still be $\sim 40\%$ of the total isometric force but, since cross-bridges only account for half of the isometric force, this would correspond to an $\sim 80\%$ increase in cross-bridge force, and a peak force of ~ 1.8. A similar amplification occurs with phase III. This latter effect is particularly important, because for the model to fit a larger phase III, it requires a larger decrease in ADP release rate, and an increase in force-dependence (i.e. a larger E). Thus, while the full stretch amplitude in these fits results in a smaller force-dependence compared to our fits with decreased stretch amplitude (compare main text Fig. 3B to Fig. S13b), this effect is mostly opposed by the large amount of unexplained force which requires larger force-dependence to fit the increased amplitude of phase III relative to isometric cross-bridge force (Fig. S13b).

23

Thus, we reject the explanation that including an unexplained force due to non-cross-bridge effects is the sole reason for the discrepancy we see between model and measurement.

7 Alternative Model Assumptions

Given the inconsistency between our measurements and our four- and five-state models, we conclude that at least one of the model assumptions is wrong. Thus, we considered the model assumptions to see if adjusting any would provide a solution to the discrepancy between model and data. We discuss these assumptions below, including the effects of non-linear elasticity of myosin, force-dependence of weak-binding kinetics and thin-filament activation. Notably, we found that none of these effects is likely to explain the discrepancy.

7.1 Non-linear Elasticity

One of the key model assumptions is that myosin acts as a linear spring with constant stiffness, κ, leading to a linear force-displacement relationship, $F(x) = \kappa x$. While there is some experimental evidence to support this assumption [27], there is also evidence to suggest that myosin's stiffness may be significantly lower when the molecule is compressed [28], leading to a non-linear force-displacement curve for myosin.

We expected that such non-linear elasticity might improve the agreement between the model and our measurements. In particular, the decreased stiffness during compression would decrease resistive drag during shortening [29], leading to higher shortening velocities. Thus, at a given value of E, this model would need a smaller ADP release rate to counteract the increase in velocity. This would result in a downward shift in the best-fit parameters of the force-velocity fits (Figs. 3B and 4B in main text). Because cross-bridge stiffness during lengthening does not change, we expected drag during lengthening to remain largely unaffected, and therefore the best-fit parameters of the force transient fits to remain the same. To test this idea, we implemented non-linear myosin elasticity in our model.

To include non-linear elasticity in the model, we defined myosin's force-displacement curve to be piecewise linear, with a much smaller slope (i.e. lower myosin stiffness) for negative displacements compared to positive displacements (Fig. S14b inset). Thus, with myosin's stiffness given by $\kappa(x)$, we get a force-displacement relationship of $F(x) = \kappa(x) \cdot x$. Additionally, in the model, myosin's probability of binding to actin with a given initial displacement depends on the negative exponential of the potential energy required to achieve that displacement (see Walcott et al. 2012 [1] for a discussion of this assumption). Therefore, since the force-extension function and the potential energy-extension function are related (the former is the negative derivative of the latter), when we modify the force-extension function to be non-linear, we must also modify the attachment rate as a function of extension.

We implement this as follows. Let $V(x)$ denote the potential energy. Since force is the negative

derivative of the potential energy, we have

$$F(x) = -\frac{dV}{dx} \quad \Rightarrow \quad V(x) = -\int F(x)dx$$

We assume that the attachment rate is the negative exponential of the potential energy. Therefore, we get the following expression for attachment rate:

$$\begin{aligned}
\kappa_w^+(x) &= k_{w_0}^+ \mathcal{C} \exp\left(-V(x)\right) \\
&= k_{w_0}^+ \mathcal{C} \exp\left(\int F(x)dx\right) \\
&= k_{w_0}^+ \mathcal{C} \exp\left(\int \kappa(x)\, x\, dx\right)
\end{aligned} \tag{24}$$

where $\mathcal{C}$ is chosen so that $\int_{-\infty}^{\infty} \kappa_w^+(x)dx = k_{w_0}^+$.

With addition of this non-linearity, the system cannot be solved analytically. Instead, we solve the system numerically, taking care to appropriately define the non-linearity as described above. To solve for the force-velocity relationship, we implement an ODE solver in Matlab (`ode15s`) and solve the system under steady-state conditions. To solve for the force transient response with stretch, we implement fourth-order Runge-Kutta to solve the system for all x, at each point in time.

Surprisingly, we found that non-linear elasticity did not improve the agreement between our model and the measurements. This lack of agreement arises from the interaction of two competing effects, 1) the expected decrease in drag, and 2) an unexpected decrease in effective power-stroke size. This latter effect arises because, when myosin's stiffness in compression is decreased, the amplitude of the thermal excursions due to Brownian motion increase. Because myosin's stiffness is asymmetric, these thermal excursions are asymmetric, making it more likely for myosin to bind with non-zero compression. Then, when the myosin molecule undergoes its power-stroke, this initial compression decreases the effective power-stroke size.

The competition between these two effects is apparent in our simulated force-velocity curves. When the decrease in stiffness for compressed myosin is small, the decrease in drag is the dominant effect. We see this as both an increase in force for a given velocity value and an increase in unloaded shortening velocity, $v_{\max}$, as we expected (Fig. S14a and inset, respectively). However, when myosin's stiffness is decreased more significantly in compression, the reduction in effective power-stroke size becomes the dominant effect. We see this as a decrease in force and unloaded shortening velocity, $v_{\max}$, compared to the previous case (Fig. S14a and inset, respectively). Thus, while non-linear myosin stiffness increases shortening rate for a given E, this effect is limited.

Additionally, although we had anticipated a minimal effect of non-linear myosin stiffness on the force transient after stretch, we observed a large effect. Non-linear myosin elasticity shifts the best-fit parameters toward a larger force-dependence at a given ADP release rate, resulting in a rightward shift in the best-fit parameters (Fig. S14b) and thus worse agreement with the best-fit force-velocity parameters. This result is due to the decrease in effective power-stroke size, which has a similar effect as decreased stretch amplitude due to series elasticity discussed earlier (section 3.2 in main text). In particular, in the model the delayed increase in force in the force transient response (phase III), arises from strongly-bound cross-bridges detaching more slowly post-stretch, due to

25
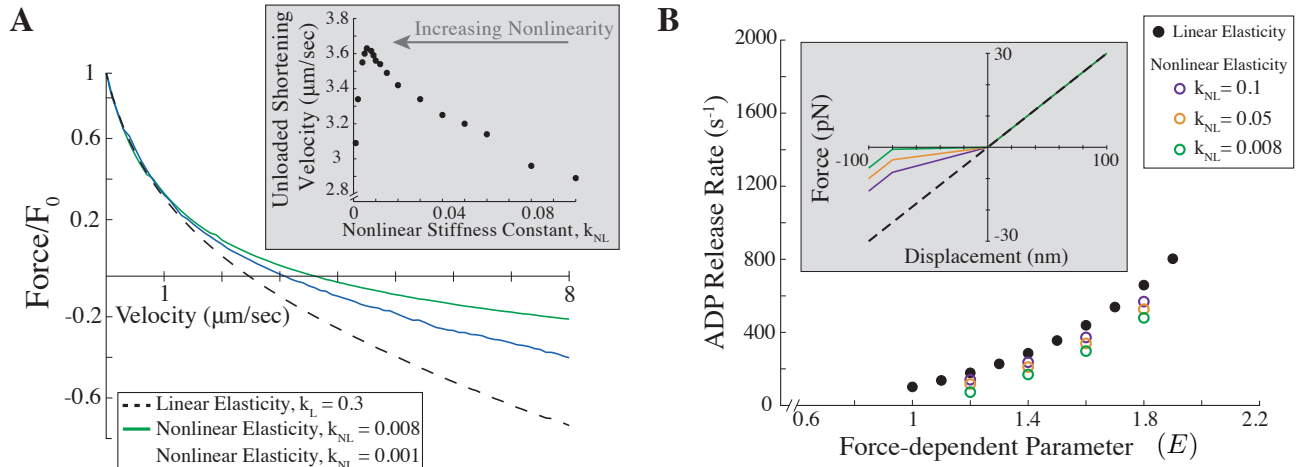
Figure S14: Non-linear elasticity of myosin does not explain the discrepancy between model and data. **A**) Force-velocity relationship for linear (dashed line) and non-linear (solid lines) cross-bridge elasticity. Inset: unloaded shortening velocity v_{max}, as a function of non-linear stiffness, illustrating that v_{max} increases and then decreases as the non-linear stiffness of myosin becomes more significant. **B**) Combinations of unloaded ADP release rate and the force-dependent parameter for linear (solid circles) and non-linear (open colored circles) cross-bridge elasticity. Inset: Force as a function of displacement for linear (dashed line) and non-linear (solid lines) cross-bridge elasticity with varying degrees of non-linearity.

the force-dependence of ADP release. The effective reduction in power-stroke size decreases the force each myosin molecule exerts and, therefore, to maintain the phase III response for non-linear elastic cross-bridges, the force dependence of ADP release must increase. We therefore conclude that non-linear myosin elasticity is unlikely to explain the difference we observe between our model and measurements.

7.2 Force-Dependent Detachment of Weakly-Bound Cross-bridges

In our original four- and five-state models, we assume that the only force-dependent rate constant is the ADP release rate. We make this assumption because the force-dependence in this transition has been directly observed and characterized (e.g. [2, 3]). However, measurements with an ultra-fast optical trap suggest additional force-dependence in the transition from a weakly-bound state to an unbound state (i.e. state 1 to state 5 in Fig. S1) [30]. To understand whether this force-dependence could explain the discrepancy between model and measurement, we explored its effect on the model.

We can gain an intuition for the effect of force-dependent detachment of weakly-bound cross-bridges by looking at a simplification of the five-state model. If weak binding is fast compared to the other state transitions, then the original five-state model (without force-dependent detachment of weakly bound cross-bridges) reduces to the four-state model with an additional viscous drag from the weakly-bound cross-bridges (Fig. S15a, see section 2). If weakly-bound cross-bridges detach more rapidly with increasing force [30], then the weakly-bound cross-bridges display shear-thinning behavior [13]. That is, the viscous drag constant decreases as shortening rate increases, leading to less drag force at higher shortening velocities (Fig. S15b).
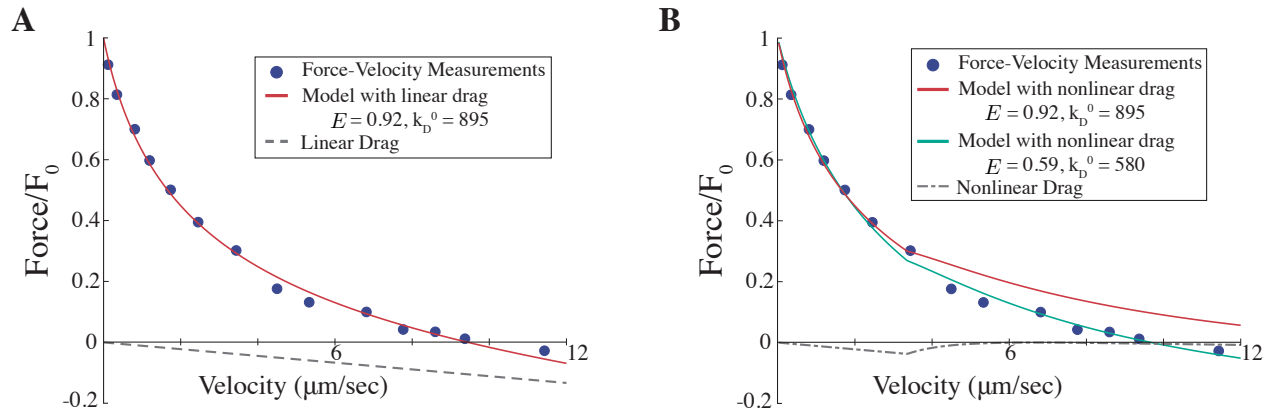
Figure S15: Force-dependent detachment of weakly-bound cross-bridges does not explain the discrepancy between model and data. **A)** Force-velocity measurements fit with the four-state model plus viscous drag. The force from weakly-bound cross-bridges is linear with velocity (dashed line). **B)** Force-velocity measurements fit with four-state model with force-dependent detachment from the weakly-bound state. The force from weakly-bound cross-bridges is decreased at higher shortening velocities (dash-dotted gray line), providing a poor fit to the measurements (red line). The model can fit the measurements with this non-linear drag (green line), but requires a smaller force-dependence and a smaller unloaded ADP release rate.

Rather than decreasing the disparity between the model parameters that generate good fits to our force-velocity and force transient measurements, such shear-thinning behavior has the opposite effect. Specifically, shear-thinning drag increases the slope of the best-fit parameters for the force-velocity data, shifting them further from the best-fit parameters for the force transient data (Figs. 3B and 4B in main text). This is because, as discussed in our model fits to Hill's measurements (Section 2.1), weakly-bound cross-bridges decrease the curvature of the force-velocity relationship. Thus, as we increase the amount of weak binding, we can generate good fits to force-velocity data with an increasing amount of force dependence (Fig. 2C in main text). Shear-thinning drag, however, is less effective in decreasing the curvature of the force-velocity curve, since the decrease in force at higher shortening velocities introduces additional curvature (Fig. S15b). Thus, fitting our force-velocity measurements with a model that includes force-dependent detachment requires less force dependence and a smaller unloaded ADP release rate, which ultimately shifts the best-fit parameters up and left, further away from the best-fit parameters for our force-transient measurements (Figs. 3B and 4B in main text). We therefore conclude that force-dependent detachment of weakly-bound cross-bridges is unlikely to explain the difference we observe between our model and measurements.
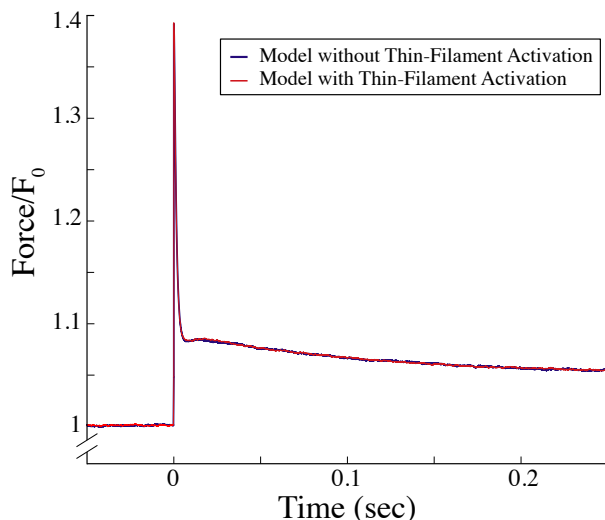
7.3 Thin-Filament Activation

Our cross-bridge models assume that one myosin's rate of strong binding (the transition from state 1 to state 2 in Fig. S1) does not depend on whether neighboring myosin are bound. This assumption would be violated if thin-filament activation contributes to the force transient response (e.g. [31]). This mechanism is thought to occur in cardiac muscle [32, 33]. Once a myosin molecule binds strongly to actin, it locally deforms the tropomyosin filament and facilitates the binding of nearby myosin (e.g. [34, 35, 36]). The longer myosin is strongly bound to actin, the greater this effect, so that under conditions of low ATP (which extends myosin's strong binding lifetime), thin

filaments can be activated at low calcium [37, 38]. If, as predicted by the model, phase III of the force transient response arises from strongly bound myosin whose attachment lifetime is prolonged due to the stretch imposed on the muscle fiber, this activation effect would amplify the response and increase phase III. In other words, if thin-filament activation contributed to phase III, then the model may be able to fit the data with a smaller force-dependence, which would then be more consistent with the force-dependence needed to fit our force-velocity measurements. It is therefore possible that the lack of this effect in the models is responsible for their inability to simultaneously fit our force-velocity and force transient measurements.

To test this idea, we implemented our five-state cross-bridge model with a previously developed model that includes thin-filament activation through local coupling of myosin molecules [34]. This model includes one key parameter, ε, that describes the rate at which a single myosin molecule binds divided by the rate at which it binds in the absence of regulation. By tuning this parameter, we can effectively change the amount of local coupling between neighboring myosin molecules. Intuitively, we expected that increasing the amount of thin-filament activation (i.e. decreasing ε) should increase the magnitude of phase III.

Unlike the differential equation simulations presented thus far, we now use a Monte Carlo simulation to implement both the activation model and our five-state cross-bridge model. In particular, we use a modified Gillespie algorithm to iterate the system throughout time, keeping track of the force produced by the myosin molecules as a function of time. We use the parameters from our five-state model best-fit to the force transient assuming the presence of an unexplained force (as in Fig. 4A of the main text), and adjust the force result to account for the non-cross-bridge force. We find that, even with an unreasonable amount of myosin coupling ($\varepsilon = 0.1$), the model gives nearly the same result with and without thin-filament activation (Fig. S16). Thus, we conclude that thin-filament activation does not play a large enough role in the force transient response to solve the disparity between fitting our two measurements.

Figure S16: Thin-filament activation does not have a significant effect on force transient results. Simulating the five-state cross-bridge model including thin-filament activation using a modified Gillespie algorithm (red line) gives nearly the same results as the five-state cross-bridge model without activation (blue line).

28

8   Model with Force-Dependent Detachment of Weakly-Bound Cross-Bridges and Series Elastic Element

To compare this model to our force transient measurements, we must numerically solve the full PDE system (Eq. 1), modified to include force-dependent unbinding from the weakly bound state, of the form

$$k_w^- = k_{w0}^- e^{E_{wb}|x|/d}$$

where E_{wb} is a non-dimensional constant that determines the force-dependence of this state. The non-dimensional parameter E_{wb} is comparable to the non-dimensional parameter E, which determines the force-dependence of ADP release. However, the sign of the x dependence for this rate constant is different from the equivalent expression for k_D, since a resisting force slows, and an assisting load accelerates ADP release, while a resisting or assisting load accelerates the detachment of weakly bound cross-bridges.

The velocity, $v(t)$, in Eq. 1 represents the velocity of actin relative to myosin. We model the series elastic element as being in series with actin. Therefore, we keep track of actin's position, x_{actin} by solving the following equation

$$x_{actin}(t) = x_{actin}(0) + \int_0^t v(\tau)d\tau$$

Then, the series elastic element applies a force $F_{SE} = \kappa_{SE}(S + L_0 - x_{actin})$, where S is the stretch applied to the system, and L_0 is the initial length of the series elastic element (such that $\kappa_{SE}L_0 = F_{iso}$). Since the spring is in series with the cross-bridges, we require that $F_{SE} = F$, where F is the force from the cross-bridges as defined by Eq. 2.

We numerically solve these equations as described in section 1.4.1 (i.e., we use the method of characteristics, and our own RK4 solver), but we must do an additional root find to find the $v(t)$ at each time step that satisfies the equation $F_{SE} = F$. We start from the initial condition described in that section, though the calculation of isometric steady state is adjusted to reflect the force-dependence of k_w^-.

To make the simulations more robust, we cutoff the value of k_w^- at $100,000$ s^{-1}. That is, at x values where $k_w^-(x) > 100,000$, we set $k_w^-(x) = 100,000$. Without this, the equations become stiff and the numerical solution unreliable. With this cutoff, the simulations were faster and more reliable. We ensured that this cutoff did not affect our simulations by doubling the cutoff (to $200,000$ s^{-1}), and ensuring that our results did not change.

We used a wide grid in x, from -20 to 20 nm, with 20,000 evenly spaced points. We simulated the model for 0.01 s, with 800 evenly spaced points. Increasing the number of points or the width of the grid did not affect our results. Increasing the time of the simulations has only a minor affect on our results and increases computational expense.

To compare this model to our force-velocity measurements, we follow the procedure described in section 1.3.1, modified to account for the force-dependence of k_w^-. The spring in series with actin does not affect these steady-state measurements.

8.1 The fits to the data

The unknown parameters in the model are the unloaded ADP release rate (k_D^0), the unloaded weak-binding detachment rate (k_{w0}^-), the weak-binding attachment rate (k_w^+) the stiffness of the series elastic element (κ_{ser}), the force-dependence of the detachment rate from the weakly-bound state (E_{wb}), and the force dependence of the detachment rate from the strongly-bound state (E). We performed fits to the data by minimizing the mean squared error to our force transient (E_t) and force-velocity (E_f) measurements. The objective function that we minimized was $E_t + 10E_f$. We weighted the error from the force-velocity measurements by a factor of 10, because in preliminary simulations where we only fit the force transient or the force-velocity measurements, the mean squared error of the best-fit to the force-velocity measurements was about 10 fold less than the mean squared error of the best-fit to the force transient measurements.

We fixed the parameters E_{wb} and E, which determine the force-dependence of unbinding from the weakly- and strongly-bound states, respectively. We then used Matlab's fminsearch function to determine the values of the other four parameters ($k_D^0, k_{w0}^-, k_w^+, \kappa_{ser}$) that optimized the fit to the data. We fixed E_{wb} and E at a several difference values (see Fig. 5D of the main text). We did not include A and E in the optimization because the reaction rates depend exponentially on these values. Therefore, if these values are not constrained, the equations can become stiff and the numerical solutions unreliable.

The optimization converged at each E, E_{wb} pair we considered. We ensured that it converged by starting each optimization from a random seed, and ensuring that each optimum discovered by the optimization was reached from at least two of these random seeds. The best-fit parameters, for $E_{wb} = 20$ and $E = 0.5$, were $k_D^0 = 1375\mathrm{s}^{-1}$, $k_{w0}^- = 505.9\mathrm{s}^{-1}$, $k_w^+ - 143.3\mathrm{s}^{-1}$ and $\kappa_{SE} = 0.000732$.

References

[1] S. Walcott, D. M. Warshaw, E. P. Debold, Mechanical coupling between myosin molecules causes differences between ensemble and single-molecule measurements, Biophysical journal 103 (3) (2012) 501–510.

[2] C. Veigel, J. E. Molloy, S. Schmitz, J. Kendrick-Jones, Load-dependent kinetics of force production by smooth muscle myosin measured with optical tweezers, Nature cell biology 5 (11) (2003) 980.

[3] N. M. Kad, J. B. Patlak, P. M. Fagnant, K. M. Trybus, D. M. Warshaw, Mutation of a conserved glycine in the sh1-sh2 helix affects the load-dependent kinetics of myosin, Biophysical journal 92 (5) (2007) 1623–1631.

[4] G. I. Bell, Models for the specific adhesion of cells to cells, Science 200 (4342) (1978) 618–627.

[5] G. I. Zahalak, A distribution-moment approximation for kinetic theories of muscular contraction, Mathematical biosciences 55 (1-2) (1981) 89–114.

[6] C. S. Newhard, S. Walcott, D. M. Swank, The load dependence of muscle's force-velocity curve is modulated by alternative myosin converter domains, American Journal of Physiology-Cell Physiology 316 (6) (2019) C844–C861.

[7] E. Eisenberg, T. L. Hill, Muscle contraction and free energy transduction in biological systems, Science 227 (4690) (1985) 999–1006.

[8] B. Brenner, Mechanical and structural approaches to correlation of cross-bridge action in muscle with actomyosin atpase in solution, Annual review of physiology 49 (1) (1987) 655–672.

[9] R. Cooke, K. C. Holmes, The mechanism of muscle contractio, Critical Reviews in Biochemistry 21 (1) (1986) 53–118.

[10] L. A. Stein, R. P. Schwarz Jr, P. B. Chock, E. Eisenberg, Mechanism of the actomyosin adenosine triphosphatase. evidence that adenosine 5'-triphosphate hydrolysis can occur without dissociation of the actomyosin complex, Biochemistry 18 (18) (1979) 3895–3909.

[11] B. Brenner, M. Schoenberg, J. Chalovich, L. Greene, E. Eisenberg, Evidence for cross-bridge attachment in relaxed muscle at low ionic strength, Proceedings of the National Academy of Sciences 79 (23) (1982) 7288–7291.

[12] B. Brenner, L. C. Yu, R. J. Podolsky, X-ray diffraction evidence for cross-bridge formation in relaxed muscle fibers at various ionic strengths, Biophysical journal 46 (3) (1984) 299–306.

[13] M. Srinivasan, S. Walcott, Binding site models of friction due to the formation and rupture of bonds: state-function formalism, force-velocity relations, response to slip velocity transients, and slip stability, Physical Review E 80 (4) (2009) 046124.

[14] A. V. Hill, The heat of shortening and the dynamic constants of muscle, Proc. R. Soc. Lond. B 126 (843) (1938) 136–195.

[15] W. O. Fenn, A quantitative comparison between the energy liberated and the work performed by the isolated sartorius muscle of the frog, The Journal of physiology 58 (2-3) (1923) 175–203.

[16] S. Galler, T. L. Schmitt, D. Pette, Stretch activation, unloaded shortening velocity, and myosin heavy chain isoforms of rat skeletal muscle fibres., The Journal of physiology 478 (3) (1994) 513–521.

[17] S. Galler, K. Hilber, D. Pette, Stretch activation and myosin heavy chain isoforms of rat, rabbit and human skeletal muscle fibres, Journal of Muscle Research & Cell Motility 18 (4) (1997) 441–448.

[18] C. R. Straight, K. M. Bell, J. N. Slosberg, M. S. Miller, D. M. Swank, A myosin-based mechanism for stretch activation and its possible role revealed by varying phosphate concentration in fast and slow mouse skeletal muscle fibers, American Journal of Physiology-Cell Physiology 317 (6) (2019) C1143–C1152.

[19] J. Ochala, D. J. Dorer, W. R. Frontera, L. S. Krivickas, Single skeletal muscle fiber behavior after a quick stretch in young and older men: a possible explanation of the relative preservation of eccentric force in old age, Pflügers Archiv 452 (4) (2006) 464–470.

[20] F. Vanzi, G. Piazzesi, M. Linari, M. Reconditi, V. Lombardi, An analysis of the tension transient after a step stretch imposed during an isometric tetanus, Biophysical journal 68 (4 Suppl) (1995) 370s.

[21] G. Piazzesi, M. Linari, M. Reconditi, F. Vanzi, V. Lombardi, Cross-bridge detachment and attachment following a step stretch imposed on active single frog muscle fibres., The Journal of physiology 498 (1) (1997) 3–15.

[22] S. Galler, K. Hilber, D. Pette, Force responses following stepwise length changes of rat skeletal muscle fibre types., The Journal of physiology 493 (1) (1996) 219–227.

[23] D. Labeit, K. Watanabe, C. Witt, H. Fujita, Y. Wu, S. Lahmers, T. Funck, S. Labeit, H. Granzier, Calcium-dependent molecular spring elements in the giant protein titin, Proceedings of the National Academy of Sciences 100 (23) (2003) 13716–13721.

[24] T. R. Leonard, W. Herzog, Regulation of muscle force in the absence of actin-myosin-based cross-bridge interaction, American Journal of Physiology-Cell Physiology 299 (1) (2010) C14–C20.

[25] R. A. Koppes, D. M. Swank, D. T. Corr, A new experimental model for force enhancement: steady-state and transient observations of the drosophila jump muscle, American Journal of Physiology-Cell Physiology 309 (8) (2015) C551–C557.

[26] S. Walcott, W. Herzog, Modeling residual force enhancement with generic cross-bridge models, Mathematical biosciences 216 (2) (2008) 172–186.

[27] M. Linari, G. Piazzesi, I. Pertici, J. A. Dantzig, Y. E. Goldman, V. Lombardi, Straightening out the elasticity of myosin cross-bridges, Biophysical Journal 118 (5) (2020) 994–1002.

[28] M. Kaya, H. Higuchi, Nonlinear elasticity and an 8-nm working stroke of single myosin molecules in myofilaments, Science 329 (5992) (2010) 686–689.

[29] R. K. Brizendine, D. B. Alcala, M. S. Carter, B. D. Haldeman, K. C. Facemyer, J. E. Baker, C. R. Cremo, Velocities of unloaded muscle filaments are not limited by drag forces imposed by myosin cross-bridges, Proceedings of the National Academy of Sciences 112 (36) (2015) 11235–11240.

[30] M. Capitanio, M. Canepari, M. Maffei, D. Beneventi, C. Monico, F. Vanzi, R. Bottinelli, F. S. Pavone, Ultrafast force-clamp spectroscopy of single molecules reveals load dependence of myosin working stroke, Nature methods 9 (10) (2012) 1013–1019.

[31] L. E. Greene, E. Eisenberg, Cooperative binding of myosin subfragment-1 to the actin-troponin-tropomyosin complex, Proceedings of the National Academy of Sciences 77 (5) (1980) 2616–2620.

[32] K. B. Campbell, M. Chandra, Functions of stretch activation in heart muscle, The Journal of general physiology 127 (2) (2006) 89–94.

[33] J. E. Stelzer, L. Larsson, D. P. Fitzsimons, R. L. Moss, Activation dependence of stretch activation in mouse skinned myocardium: implications for ventricular function, The Journal of general physiology 127 (2) (2006) 95–107.

[34] T. Longyear, S. Walcott, E. P. Debold, The molecular basis of thin filament activation: from single molecule to muscle, Scientific Reports 7 (1) (2017) 1822.

[35] R. Craig, W. Lehman, Crossbridge and tropomyosin positions observed in native, interacting thick and thin filaments, Journal of molecular biology 311 (5) (2001) 1027–1036.

[36] D. McKillop, M. A. Geeves, Regulation of the interaction between actin and myosin sub-fragment 1: evidence for three states of the thin filament, Biophysical journal 65 (2) (1993) 693–701.

[37] R. D. BREMEL, A. WEBER, Cooperation within actin filament in vertebrate skeletal muscle, Nature New Biology 238 (82) (1972) 97–101.

[38] N. M. Kad, S. Kim, D. M. Warshaw, P. VanBuren, J. E. Baker, Single-myosin crossbridge interactions with actin filaments regulated by troponin-tropomyosin, Proceedings of the National Academy of Sciences 102 (47) (2005) 16990–16995.